J. Fluid Mech. (1992), *vol.* 237, *pp.* 231–260
Printed in Great Britain

Distortion of a flat-plate boundary layer by free-stream vorticity normal to the plate

By M. E. GOLDSTEIN[1], S. J. LEIB[2] AND S. J. COWLEY[3]

[1] Lewis Research Center, Cleveland, OH 44135, USA

[2] Sverdrup Technology, Inc. Lewis Research Center Group, Brook Park, OH 44142, USA

[3] Department of Applied Mathematics and Theoretical Physics, University of Cambridge, Silver Street, Cambridge CB3 9EW, UK

(Received 12 October 1990 and in revised form 20 September 1991)

We consider a nominally uniform flow over a semi-infinite flat plate. Our analysis shows how a small streamwise disturbance in the otherwise uniform flow ahead of the plate is amplified by leading-edge bluntness effects and eventually leads to a small-amplitude but nonlinear spanwise motion far downstream from the leading edge of the plate. This spanwise motion is then imposed on the viscous boundary-layer flow at the surface of the plate – causing an order-one change in its profile shape. This ultimately reduces the wall shear stress to zero – causing the boundary layer to undergo a localized separation, which may be characterized as a kind of bursting phenomenon that could be related to the turbulent bursts observed in some flat-plate boundary-layer experiments.

1. Introduction

Much of our information about boundary-layer phenomena derives from experimental measurements made in flows over relatively thin flat plates embedded in nominally uniform free streams. Such experiments are attempts to simulate the flow over an infinitely thin flat plate embedded in a completely uniform stream and it is important to know how relatively small imperfections in the experimental environment can affect the final measured results.

This paper shows how small, but steady, variations in the upstream velocity field can produce somewhat larger streamwise vorticity fields which can, in turn, produce significant (i.e. order-one) variations in the streamwise boundary-layer profiles. These variations could, for example, be quite important in the boundary-layer transition experiments, which are frequently conducted with flow configurations of the type being considered herein. In fact, there are many experiments of this type in which instability wave growth is found to occur upstream of the theoretical (i.e. two-dimensional flat-plate) lower branch of the neutral stability curve or in which the observed instability wave growth rates exceed the theoretical values. Some of these observations may, in part, be explained by the present results which show that the free-stream disturbances cause the local wall shear to become very small at certain discrete spanwise locations. This could easily move the lower branch of the neutral stability curve upstream, or at least augment the local growth rate of the instability waves and thereby explain some of the experimental observations. These issues, while quite interesting, are not pursued in the present work which concentrates on understanding the basic steady flow.

Crow (1966) also considered the steady distortion of flat-plate boundary-layer flows by free-stream non-uniformities, but that work is quite different from ours. This is mainly due to a difference in the basic scaling that allows our free-stream disturbances to become fully nonlinear before viscous effects can set in. This, in turn, has an important effect on the subsequent development of the flow and leads to an asymptotic solution that explicitly exhibits some interesting features of the motion which would otherwise be obscured by viscous phenomena. In this regard, it is worth noting that leading-edge bluntness effects play a central role in the present work, while Crow (1966) is able to consider an infinitely thin flat plate.

We assume that the characteristic dimension of the rounded leading edge is of the order of the spanwise lengthscale, say λ, of the upstream disturbance field, and that the Reynolds number based on λ, say R_λ, is large. Then the upstream distortion interacts linearly with the leading edge with the resulting flow being well described by the usual 'rapid distortion' theory (Hunt & Carruthers 1990; Goldstein 1978). The relevant analysis was, at least in principle, given by Lighthill (1956) who showed that the upstream distortion produces a crossflow velocity field that becomes logarithmically infinite at the surface of the body. This singularity must ultimately be removed by viscous effects, which (as in Toomre 1960) are confined to the viscous boundary-layer region (with the Reynolds number–amplitude scaling being considered herein). Our analysis shows that inviscid crossflow effects produce only a linear perturbation to the boundary-layer flow in the vicinity of the leading edge, where the undisturbed boundary layer undergoes its most rapid streamwise development, but that they produce an order-one change in the mean boundary-layer profiles at large distances downstream where its streamwise development is on a considerably slower scale.

However, the linear rapid-distortion-theory solution, which provides an adequate description of the external inviscid flow in the vicinity of the leading edge, breaks down at large streamwise distances, with the breakdown moving further upstream as the surface of the plate is approached. A new nonlinear solution then has to be obtained in order to describe the external inviscid flow in the physically interesting region where crossflow effects produce significant (i.e. order-one) changes in the boundary-layer profiles. The thickness of this nonlinear inviscid region is small compared to its streamwise dimension but large compared to the boundary-layer thickness. It serves as a kind of 'blending layer' that connects the boundary-layer solution to the linear rapid-distortion-theory solution, which applies at an order-one (on the scale of λ) distance from the wall.

The blending-layer flow is governed by the inviscid Burgers' equation (sometimes called the kinematic wave equation) whose solution eventually develops a singularity at a certain spanwise location and at a finite downstream position owing to the well-known wave steepening effects associated with that solution. This also leads to a singularity (signified by the vanishing of the wall shear) in the boundary-layer flow at the same (spanwise and streamwise) location.

New local solutions to the blending and boundary-layer problems have to be worked out in order to describe the structure of these regions. We show that the two solutions can be matched in an appropriate overlap domain. The boundary-layer solution actually develops a double-layer structure as it approaches the singularity so that the overall asymptotic structure has three layers in the vicinity of the singularity. The main purpose of this paper is to investigate the relevant structure of this local solution.

The overall plan of the paper is as follows. Section 2.1 describes the linear inviscid

flow produced by the steady upstream distortion field and the initial breakdown of the relevant linear 'rapid-distortion' theory solution is discussed in §2.2. The appropriate nonlinear, but inviscid, solution that eliminates the breakdown is described in §3. In §4 we show that this solution develops a line singularity somewhat further downstream and that this singularity can, in turn, be eliminated by a new local solution to the problem.

The viscous boundary-layer problem is formulated in §5. The solution to this problem develops a singularity at the position of the inviscid singularity and the terminal form of the boundary-layer solution is worked out in §5.2. This local similarity solution has a double layer structure with an outer inviscid region and a viscous wall layer. A new expansion which applies in the vicinity of the singularity is worked out in §5.3. This solution has the same streamwise lengthscale as the external solution and it is shown that the two solutions can be matched in an appropriate overlap domain.

The numerical solutions to the boundary-layer problem are described in §6. They show that it exhibits a rapid thickening in the vicinity of the singularity, which might be characterized as a kind of 'bursting' of the boundary layer – a phenomenon which has, up to now, primarily been associated with unsteady flows. This might lead to a local breakdown of the laminar boundary layer and thereby provide a possible mechanism for by-pass transition. These and other issues are discussed in §7.

2. Formulation and breakdown of linear solution

We are concerned with the flow over a semi-infinite flat plate of finite thickness h^* with leading edge 'ellipse' of dimension $O(t^*)$ (see figure 1). The upstream flow is assumed to be nominally uniform, except for a small $O(\epsilon)$ steady perturbation, say $\epsilon U_\infty u_\infty(z)$, in the streamwise velocity that depends only on the spanwise coordinate λz and has a characteristic lengthscale λ; $u_\infty(z)$ is an order-one quantity. We normalize all lengths by λ and the velocity $\boldsymbol{u} = \{u, v, w\}$ is normalized by the uniform upstream mean flow velocity U_∞. The flow is assumed to be incompressible, with density ρ. The pressure p is normalized by ρU_∞^2. The plate thickness h^* is, for simplicity, taken to be $O(\lambda)$, and the x-coordinate is assumed to be in the streamwise direction with the origin at the leading edge while the origin of the y-coordinate coincides with the flat surface of the plate far downstream in the flow.

Finally, we require that the Reynolds number $R_\lambda = U_\infty \lambda/\nu$, where ν is the kinematic viscosity, be large enough to ensure that the viscous effects are initially confined to a thin boundary layer at the surface of the plate that is predominantly two dimensional near the forward stagnation point. This will occur (and the boundary layer will then remain thin until nonlinear effects influence the external motion far downstream in the flow) if

$$\ln R_\lambda \ll \frac{1}{\epsilon} \ll R_\lambda, \tag{2.1}$$

which we now assume to be the case.

2.1. *The linear solution*

Then the entire flow is nearly two dimensional in the vicinity of the leading edge, i.e. in the region where $x = O(1)$, with the three-dimensional effects being an $O(\epsilon)$ perturbation of the two-dimensional basc flow, say $\{U_0(x, y), V_0(x, y), 0\}$. The viscous

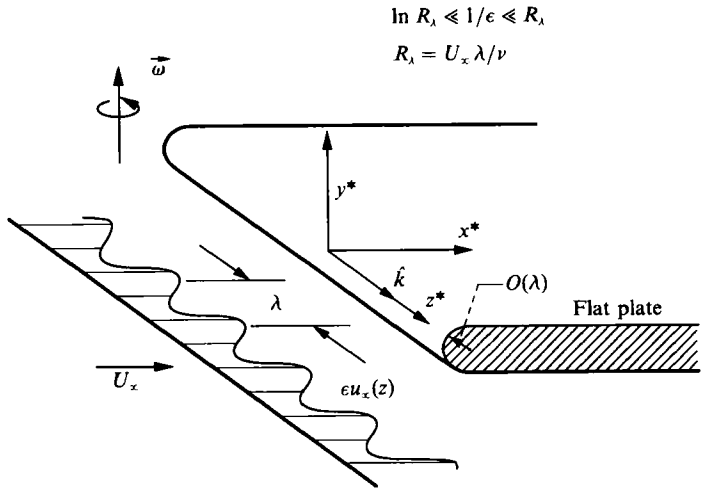

FIGURE 1. Flow configuration.

effects are confined to a thin region whose thickness is $O(R_\lambda^{-\frac{1}{2}})$. The solution outside this region should therefore expand like

$$\boldsymbol{u} = \{U_0, V_0, 0\} + \epsilon\{u_0, v_0, w_0\} + \epsilon^2\{u_1, v_1, w_1\} + \ldots = \{U_0, V_0, 0\} + \epsilon\boldsymbol{u}_0 + \epsilon^2\boldsymbol{u}_1 + \ldots, \tag{2.2}$$

$$p = P_0 + \epsilon p_0 + \epsilon^2 p_1 + \ldots. \tag{2.3}$$

The complex conjugate mean flow velocity $\zeta = U_0 - \mathrm{i}V_0$ (which is assumed to include the $O(R_2^{-\frac{1}{2}})$ boundary layer displacement effects) is an analytic function of $Z = x + \mathrm{i}[y + (h^*/\lambda)]$ that can be expressed in terms of a complex potential, say

$$\tilde{W} = \Phi + \mathrm{i}\Psi, \tag{2.4}$$

where Φ is the velocity potential and Ψ is the stream function, in the usual way by

$$\zeta = \frac{\mathrm{d}\tilde{W}}{\mathrm{d}Z}. \tag{2.5}$$

For definiteness, we suppose that $\Psi = 0$ on the surface of the (body) plate and along the stagnation streamline, and that $\Phi \to 0$ at the forward stagnation point.

The first-order perturbations are governed by the linearized Euler equations and the results obtained by Goldstein (1978) (also see Goldstein 1979) can readily be specialized to the present case to show that the relevant solution can be written as

$$\boldsymbol{u}_0 = \nabla\phi + u_\infty(z)\,\nabla\Delta(x, y), \tag{2.6}$$

$$p_0 = -\left(U_0\frac{\partial}{\partial x} + V_0\frac{\partial}{\partial y}\right)\phi, \tag{2.7}$$

where

$$\nabla^2\phi = -u_\infty(z)\,\nabla^2\Delta, \tag{2.8}$$

$$\Delta = \Phi + \int_{-\infty}^{\Phi}\left[\frac{1}{U_0^2(\Psi, \tilde{\Phi}) + V_0^2(\Psi, \tilde{\Phi})} - 1\right]\mathrm{d}\tilde{\Phi} \tag{2.9}$$

is the Lighthill (1956)–Darwin (1954) drift function, and the normal component of $\boldsymbol{u}_0$ must vanish at the surface of the plate.

2.2. *Breakdown of the linear solution*

The expansions (2.1) and (2.3) are non-uniform in the vicinity of the plate. In fact, it follows from these equations, along with the results of the Appendix, that the crossflow velocity w_0 becomes infinite there like

$$w_0 \to \frac{u'_\infty(z)}{a} \ln \Psi \quad \text{as} \quad \Psi \to 0, \tag{2.10}$$

where a is a constant related to the local potential flow behaviour in the vicinity of the forward stagnation point and the prime denotes differentiation with respect to z (also see Lighthill 1956). The remaining velocity components, as well as the pressure, remain finite. The strongest non-uniformity occurs in the stagnation-point region where the mean flow goes to zero. In fact, it follows from the results of the Appendix that ϵp_0 becomes of the same order as P_0 at an $O(\epsilon^{\frac{1}{2}})$ distance from this point. However, the linearized equations still give the correct solution (to the order of interest here) right up to the edge of the viscous boundary layer and this non-uniformity need not be considered further.

However, another, much more important, non-uniformity develops far downstream in the flow where x becomes large. To understand its structure we note that as $x \to \infty$

$$\Psi \to y, \quad U_0 \to 1, \quad \Phi \to x, \quad \Delta \to \Delta_+(y) + x, \tag{2.11}$$

where

$$\Delta_+(y) = \int_{-\infty}^{\infty} \left(\frac{1}{U_0^2 + V_0^2} - 1 \right) \mathrm{d}\Phi \to \Delta_0(y) - \frac{1}{a} \ln y \quad \text{as} \quad y \to 0 \tag{2.12}$$

and Δ_0 remains bounded as $y \to 0$.

We now suppose that x is large and introduce the new dependent variable

$$\tilde{\phi} \equiv \phi + u_\infty(z)\, \Delta_+(y). \tag{2.13}$$

Equations (2.6) and (2.8) then show that

$$\nabla^2 \tilde{\phi} = u''_\infty \Delta_+, \tag{2.14}$$

and the normal component of $\boldsymbol{u}_0$ will vanish at the plate if

$$\frac{\partial \tilde{\phi}}{\partial y} = 0 \quad \text{at} \quad y = 0. \tag{2.15}$$

It now follows from (2.12) and (2.15) that $\tilde{\phi}$ becomes independent of x and, consequently, that (see (2.7))

$$\boldsymbol{u}_0 \to \left(u_\infty, \frac{\partial \tilde{\phi}}{\partial y}, \frac{\partial \tilde{\phi}}{\partial z} - u'_\infty \Delta_+ \right), \tag{2.16}$$

$$p_0 \to 0, \tag{2.17}$$

and

$$\tilde{\phi} \to \beta(z) - \frac{u''_\infty}{a} \frac{y^2}{2} \ln y \quad \text{as} \quad y \to 0. \tag{2.18}$$

Substituting (2.2) and (2.3) into Euler's equations and using the second member of (2.11) along with (2.14) shows that

$$\frac{\partial \boldsymbol{u}_1}{\partial x} + \nabla p_1 \to -\boldsymbol{u}_0 \cdot \nabla \boldsymbol{u}_0 \to -\left[\tilde{\phi}_y \frac{\partial}{\partial y} + (\tilde{\phi}_z - u'_\infty \Delta_+) \frac{\partial}{\partial z} \right] (u_\infty, \tilde{\phi}_y, \tilde{\phi}_z - u'_\infty \Delta_+) \quad \text{as} \quad x \to \infty. \tag{2.19}$$

It therefore follows from (2.12) and (2.18) that

$$\frac{\partial}{\partial x}(u_1+p_1)\to-\frac{u_\infty'^{\,2}}{a}\ln y, \tag{2.20}$$

$$\frac{\partial v_1}{\partial x}+\frac{\partial p_1}{\partial y}\to-\frac{(u_\infty''^{\,2}-u_\infty' u_\infty''')}{a^2}y\ln^2 y, \tag{2.21}$$

$$\frac{\partial w_1}{\partial x}+\frac{\partial p_1}{\partial z}\to-\frac{u_\infty' u_\infty''}{a^2}\ln^2 y \quad \text{as} \quad x\to\infty, \quad y\to 0. \tag{2.22}$$

Then since $\boldsymbol{u}_1$ satisfies the continuity equation

$$\nabla\cdot\boldsymbol{u}_1=0, \tag{2.23}$$

it follows from these results that

$$\nabla^2 p_1\to-2\left(\frac{u_\infty''}{a}\ln y\right)^2 \quad \text{as} \quad y\to 0, \quad x\to\infty, \tag{2.24}$$

and, consequently, that

$$p_1\to \mathrm{d}(z)-\left(\frac{u_\infty'' y\ln y}{a}\right)^2 \quad \text{as} \quad y\to 0, \quad x\to\infty. \tag{2.25}$$

It now follows from (2.2), (2.3), (2.10), (2.11), (2.16), (2.17) and (2.20)–(2.22) that

$$u\to 1+\epsilon u_\infty(z)-\frac{\epsilon^2 x u_\infty'^{\,2}}{a}\ln y, \tag{2.26}$$

$$w\to\frac{\epsilon u_\infty'}{a}\ln y-\frac{\epsilon^2 x u_\infty' u_\infty''}{a^2}\ln^2 y, \tag{2.27}$$

$$p\to\epsilon^2\mathrm{d}(z)-\left(\frac{\epsilon u_\infty'' y\ln y}{a}\right)^2, \tag{2.28}$$

as $x\to\infty$, $y\to 0$.

It is clear that this linear expansion must break down when

$$-\epsilon x\ln y=O(1) \tag{2.29}$$

and that a new solution must then be found for this region.

3. Blending-layer solution

To obtain this solution we anticipate that viscous effects will still be unimportant and introduce the new gauge functions $\sigma(\epsilon)$ and $\delta(\epsilon)$, where (see also (5.4))

$$\sigma(\epsilon)=-\frac{1}{\ln\delta(\epsilon)}\to 0 \quad \text{as} \quad \epsilon\to 0, \tag{3.1}$$

along with the new scaled variables

$$\bar{x}\equiv\frac{\epsilon x}{\sigma} \tag{3.2}$$

and

$$\eta\equiv-\sigma\ln y=\frac{\ln y}{\ln\delta}. \tag{3.3}$$

The necessity of using logarithmic variables in problems of this type was pointed out by Lagerstrom & Casten (1972) and by Bush (1971) (see also Agrawal & Messiter 1984).

We simplify the algebra by using the new independent variables

$$\xi \equiv \bar{x}\eta \tag{3.4}$$

and η in place of $\bar{x}$ and η. Then the Euler and continuity equations become

$$\left[\frac{\epsilon}{\sigma}\eta u\frac{\partial}{\partial\xi}-\sigma v\,\mathrm{e}^{\eta/\sigma}\left(\frac{\partial}{\partial\eta}+\frac{\xi}{\eta}\frac{\partial}{\partial\xi}\right)+w\frac{\partial}{\partial z}\right]\boldsymbol{u}=-\left[\frac{\epsilon}{\sigma}\eta\frac{\partial}{\partial\xi},\,-\sigma\,\mathrm{e}^{\eta/\sigma}\left(\frac{\partial}{\partial\eta}+\frac{\xi}{\eta}\frac{\partial}{\partial\xi}\right),\frac{\partial}{\partial z}\right]p, \tag{3.5}$$

and

$$\frac{\epsilon}{\sigma}\eta\frac{\partial u}{\partial\xi}-\sigma\,\mathrm{e}^{\eta/\sigma}\left(\frac{\partial}{\partial\eta}+\frac{\xi}{\eta}\frac{\partial}{\partial\xi}\right)v+\frac{\partial w}{\partial z}=0. \tag{3.6}$$

Equations (2.26)–(2.28) suggest that the solution in this region will be of the form

$$u=1+\epsilon[\bar{u}_0(\xi,z)+\sigma\frac{\xi}{\eta}\bar{u}_1(\xi,z)+\dots], \tag{3.7}$$

$$v=\frac{\epsilon}{\sigma}\mathrm{e}^{-\eta/\sigma}[\eta\bar{v}_0(\xi,z)+\sigma\bar{v}_1(\xi,z)+\dots], \tag{3.8}$$

$$w=\frac{\epsilon}{\sigma}[\eta\bar{w}_0(\xi,z)+\sigma\bar{w}_1(\xi,z)+\dots], \tag{3.9}$$

and

$$p=\epsilon^2\mathrm{d}(z)+\frac{1}{2}\left(\frac{\epsilon}{\sigma}\mathrm{e}^{-\eta/\sigma}\right)^2[\eta^2\bar{p}_0(\xi,z)+\sigma\eta\bar{p}_1(\xi,z)+\dots], \tag{3.10}$$

where $\bar{u}_0,\bar{u}_1,\bar{v}_0,\bar{v}_1,\bar{w}_0$, etc. are, of course, assumed to remain $O(1)$ in the 'blending layer' limit $\epsilon\to0$ with ξ,η,z held fixed.

Substituting these into (3.5) and (3.6) and retaining only lowest-order terms, we obtain

$$\frac{\partial\bar{u}_0}{\partial\xi}+\bar{w}_0\frac{\partial\bar{u}_0}{\partial z}=0, \tag{3.11}$$

$$\frac{\partial\bar{v}_0}{\partial\xi}+\bar{v}_0^2+\bar{w}_0\frac{\partial\bar{v}_0}{\partial z}=-\bar{p}_0, \tag{3.12}$$

$$\frac{\partial\bar{w}_0}{\partial\xi}+\bar{w}_0\frac{\partial\bar{w}_0}{\partial z}=0, \tag{3.13}$$

and

$$\bar{v}_0+\frac{\partial\bar{w}_0}{\partial z}=0, \tag{3.14}$$

respectively. Equation (3.13) can be solved for $\bar{w}_0$, and the result can be used in (3.14) to determine $\bar{v}_0$, which can, in turn, be used in (3.12) to determine $\bar{p}_0$. In fact, substituting (3.14) into (3.12) and using (3.13) shows that

$$\bar{p}_0=-2\left(\frac{\partial\bar{w}_0}{\partial z}\right)^2=-2\bar{v}_0^2. \tag{3.15}$$

Equation (3.11) can, of course, be solved for $\bar{u}_0$.

It is well known that the general solution to the kinematic wave equation (3.13) can be written implicitly as

$$\bar{w}_0 = F(z-\bar{w}_0\xi), \tag{3.16}$$

where F is an, as yet, undetermined (i.e. arbitrary) function of the indicated argument. This solution must match onto the linear solution (2.27) in the limit as $\eta \to 0$ with $\bar{x}$ fixed, and in the limit $\bar{x} \to 0$ with η fixed – both of which correspond to the limit $\xi \to 0$.

Expanding (3.16) for small ξ, we obtain

$$\bar{w}_0 = F(z) - F'(z)F(z)\eta\bar{x} + \ldots. \tag{3.17}$$

It therefore follows from (3.2) and (3.3) that (3.9) becomes identical to (2.27) when F is taken to be

$$F(z) = -\frac{u'_\infty(z)}{a}. \tag{3.18}$$

Equations (3.3) and (3.4) show that $\xi = \bar{x}(1-\sigma \ln \bar{y})$ so that in the 'small' sublayer

$$\bar{y} \equiv \frac{y}{\delta} = O(1) \tag{3.19}$$

of the much thicker region $\eta = O(1)$, (3.16) becomes

$$\bar{w}_0 = F(z-\bar{x}\bar{w}_0) \quad \text{for} \quad \bar{y} = O(1). \tag{3.20}$$

At next order we find that $\bar{w}_1$ satisfies

$$\frac{\partial \bar{w}_1}{\partial \xi} + \bar{w}_0 \frac{\partial \bar{w}_1}{\partial z} + \bar{w}_1 \frac{\partial \bar{w}_0}{\partial z} = \bar{v}_0\left(\bar{w}_0 + \xi \frac{\partial \bar{w}_0}{\partial \xi}\right) = -\bar{w}_0 \frac{\partial \bar{w}_0}{\partial z}\left(1 - \xi \frac{\partial \bar{w}_0}{\partial z}\right), \tag{3.21}$$

where we have used (3.13) and (3.14) to obtain the last member. This equation possess the general solution

$$\bar{w}_1 = \bar{w}_0[\bar{w}_{0z}\bar{G}(z-\bar{w}_0\xi) + (1-\xi\bar{w}_{0z})\ln|\bar{w}_{0z}|], \tag{3.22}$$

where $\bar{G}$ is an arbitrary function of the indicated argument that is determined by matching with the upstream linear solution of §2.1. In fact it follows from (2.2), (2.12), (2.16), (2.18) and (2.27) that $\bar{G}$ is given by

$$\bar{G}(z) = -a\frac{a\Delta_0(0) - a\gamma(z) - \ln|u''_\infty(z)/a|}{u''_\infty(z)}, \tag{3.23}$$

where we have put

$$\gamma(z) \equiv \frac{\beta'(z)}{u'_\infty(z)}. \tag{3.24}$$

4. Removal of infinite singularity

It is well known that the kinematic wave solution (3.16) does not remain valid for all $\xi > 0$. In fact, differentiating (3.16), with respect to z, shows that

$$\frac{\partial \bar{w}_0}{\partial z} = \frac{F'}{1+\xi F'}, \tag{4.1}$$

which becomes singular at $\xi = -1/F'$. Here, the prime denotes differentiation with

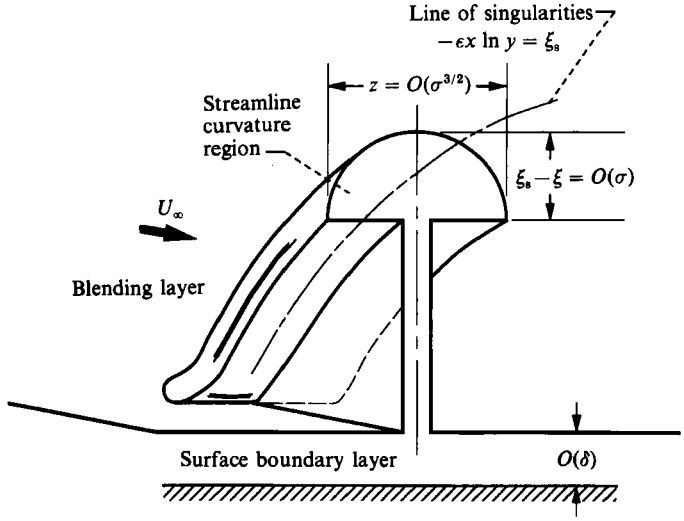

FIGURE 2. Inviscid singularity structure.

respect to the entire argument. The initial singularity (if there is more than one) occurs at the downstream location, say ξ_s, given by

$$\xi_s = \operatorname*{Min}_{\zeta} \bar{g}(\zeta), \tag{4.2}$$

where

$$\bar{g}(\zeta) \equiv -\frac{1}{F'(\zeta)}, \tag{4.3}$$

which means that $\bar{g}' = F''/F'^2$ should equal zero and F''' should be positive there (see figure 2). We denote the corresponding value of z by z_s. The solution becomes multiple valued for $\xi > \xi_s$ but can be made single valued by allowing $\bar{w}_0$ to be discontinuous across the downstream portion of an appropriate surface which reduces to the $z = z_s$ plane for the symmetric flow discussed below.

Then since we can always assume that $F(\zeta)$, as defined by (3.18), is an analytic function of ζ, this quantity can certainly be expanded in a Taylor series about $w_s, z_s, \xi_s = -1/F'(\zeta_s)$ to obtain

$$\frac{1}{\xi_s}[z - z_s - w_s(\xi - \xi_s) - (\bar{w}_0 - w_s)(\xi - \xi_s)] + \frac{\xi_s^3}{3!}F'''(\zeta_s)(\bar{w}_0 - w_s)^3 + \ldots = 0, \tag{4.4}$$

which can be solved for $\bar{w}_0 - w_s$ to obtain

$$\bar{w}_0 - w_s = \beta_s^3 \left(\frac{\xi_s - \xi}{3}\right)^{\frac{1}{2}} B(\chi) + \ldots, \tag{4.5}$$

where we have put

$$\chi \equiv \frac{3^{\frac{3}{2}}[z_s - z - w_s(\xi_s - \xi)]}{2[\beta_s(\xi_s - \xi)]^{\frac{3}{2}}}, \tag{4.6}$$

$$\beta_s^3 = \frac{3!}{\xi_s^4 F'''(\zeta_s)}, \tag{4.7}$$

and B, which is given by

$$B(\zeta) \equiv [(\zeta^2 + 1)^{\frac{1}{2}} + \zeta]^{\frac{1}{3}} - [(\zeta^2 + 1)^{\frac{1}{2}} - \zeta]^{\frac{1}{3}} \tag{4.8}$$

for real ζ, is determined by the cubic equation

$$B^3+3B-2\zeta=0 \tag{4.9}$$

for any (real or complex) value of ζ.

Equations (3.14) and (4.5)–(4.9) describe the singularity structure of $\bar{v}_0$ and $\bar{w}_0$ at the point ξ_s, z_s. We now construct an appropriate local solution that removes the infinite singularity in $\bar{v}_0$. We can suppose, without loss of generality, that the singularity occurs at $z_s=0$ and, for definiteness, we consider only the case, corresponding to our numerical example, where $z=0$ is a symmetry plane and w_s is therefore equal to zero. Then $\beta'(z)$ will be an odd function of z which vanishes at $z=0$, which means that $\gamma(z)$ remains finite there.

Expanding (4.8) for small ζ and using (3.9), (3.22), (4.1) and (4.5) we find that

$$w=\frac{\epsilon\eta z}{\sigma(\xi-\xi_s)}\left\{1+\frac{1}{(\xi-\xi_s)}\left[\frac{z}{\beta_s^{\frac{3}{2}}(\xi-\xi_s)}\right]^2\right\}+\frac{\epsilon\xi_s z}{(\xi-\xi_s)^2}[\xi_\Delta+\ln(\xi_s-\xi)]+\ldots, \tag{4.10}$$

where we have put

$$\xi_\Delta\equiv\frac{\bar{G}(0)}{\xi_s}. \tag{4.11}$$

The first significantly different scaling occurs when

$$\bar{\xi}\equiv\frac{\eta(\xi-\xi_s)}{\sigma\xi_s}-\ln\left(\frac{\xi_s\sigma}{\eta}\right)=O(1), \tag{4.12}$$

where we inserted the $\ln\sigma$ shift in the singularity position to facilitate matching logarithmic terms.

Then (4.6) shows that the appropriate 'z-scaling' is

$$\bar{z}=\left(\frac{\eta}{\sigma\beta_s\xi_s}\right)^{\frac{3}{2}}z=O(1), \tag{4.13}$$

and that the dependent variables should scale like

$$u=1+O(\epsilon) \tag{4.14}$$

$$v=\frac{\epsilon}{\sigma^2\xi_s}e^{-\eta/\sigma}\eta^2\bar{v}_I(\bar{\xi},\bar{z})+\ldots, \tag{4.15}$$

$$w=\epsilon\left(\frac{\xi_s\beta_s^3\eta}{\sigma}\right)^{\frac{1}{2}}\bar{w}_I(\bar{\xi},\bar{z})+\ldots, \tag{4.16}$$

and

$$p=\epsilon^2 d(0)+\frac{1}{2}\left(\frac{\epsilon\eta^2}{\sigma^2\xi_s}e^{-\eta/\sigma}\right)^2\bar{p}_I(\bar{\xi},\bar{z})+\ldots, \tag{4.17}$$

where $\bar{v}_I$, $\bar{w}_I$, and $\bar{p}_I$ remain of order one in the limit as $\epsilon\to 0$ with $\bar{\xi}$, η, and $\bar{z}$ held fixed. Substituting into (3.5) and (3.6) and retaining only the lowest-order terms now yields

$$(1-\bar{v}_I)\frac{\partial\bar{v}_I}{\partial\bar{\xi}}+\bar{v}_I^2+\bar{w}_I\frac{\partial\bar{v}_I}{\partial\bar{z}}=-\bar{p}_I+\frac{1}{2}\frac{\partial\bar{p}_I}{\partial\bar{\xi}}, \tag{4.18}$$

$$(1-\bar{v}_I)\frac{\partial\bar{w}_I}{\partial\bar{\xi}}+\bar{w}_I\frac{\partial\bar{w}_I}{\partial\bar{z}}=0, \tag{4.19}$$

and
$$\bar{v}_{\mathrm{I}}-\frac{\partial \bar{v}_{\mathrm{I}}}{\partial \bar{\xi}}+\frac{\partial \bar{w}_{\mathrm{I}}}{\partial \bar{z}}=0, \tag{4.20}$$

which clearly generalizes (3.11)–(3.14). The new terms are, in the main, due to singularity line curvature effects. Notice that the spanwise and vertical velocity fields are now fully coupled.

Eliminating $\bar{v}_{\mathrm{I}}$ between (4.19) and (4.20) we obtain

$$\frac{\partial \bar{w}_{\mathrm{I}}}{\partial \bar{\xi}}\left(\frac{\partial \bar{w}_{\mathrm{I}}}{\partial \bar{\xi}}+\bar{w}_{\mathrm{I}}\frac{\partial \bar{w}_{\mathrm{I}}}{\partial \bar{z}}\right)+\bar{w}_{\mathrm{I}}\left(\frac{\partial \bar{w}_{\mathrm{I}}}{\partial \bar{z}}\frac{\partial^2 \bar{w}_{\mathrm{I}}}{\partial \bar{\xi}^2}-\frac{\partial \bar{w}_{\mathrm{I}}}{\partial \bar{\xi}}\frac{\partial^2 \bar{w}_{\mathrm{I}}}{\partial \bar{\xi}\,\partial \bar{z}}\right)=0. \tag{4.21}$$

The solution to this equation must match onto the inner expansion of the outer solution in some overlap domain. We therefore require that

$$\bar{w}_{\mathrm{I}}\rightarrow-\left(-\frac{\bar{\xi}}{3}\right)^{\frac{1}{2}}B\left(\frac{3^{\frac{3}{2}}\bar{z}}{2(-\bar{\xi})^{\frac{3}{2}}}\right), \tag{4.22}$$

as $\bar{\xi}\rightarrow-\infty$ (and probably even as $\bar{\xi}\rightarrow+\infty$) and/or $\bar{z}\rightarrow\pm\infty$, with $\bar{z}/\bar{\xi}^{\frac{3}{2}}\geqslant O(1)$ and

$$\bar{w}_{\mathrm{I}}\rightarrow\frac{\bar{z}}{\bar{\xi}}\left\{1+\frac{1}{\bar{\xi}}\left[\xi_{\Delta}+\left(\frac{\bar{z}}{\bar{\xi}}\right)^2+\ln\left(-\bar{\xi}\right)\right]\right\}\quad\text{as}\quad\bar{\xi}\rightarrow-\infty\quad\text{with}\quad\frac{\bar{z}}{\bar{\xi}}=O(1). \tag{4.23}$$

Using Monge's procedure (Ames 1965, pp. 58–65) we find the first integral of (4.21) to be (this result is most easily verified by direct substitution)

$$\bar{w}_{\mathrm{I}}=G_{\mathrm{I}}\left(\bar{z}-\bar{w}_{\mathrm{I}}\left(\bar{\xi}+\ln\left|\frac{\partial \bar{w}_{\mathrm{I}}}{\partial \bar{\xi}}\right|\right)\right), \tag{4.24}$$

or equivalently

$$\bar{z}-\bar{w}_{\mathrm{I}}\left(\bar{\xi}+\ln\left|\frac{\partial \bar{w}_{\mathrm{I}}}{\partial \bar{\xi}}\right|\right)=g_{\mathrm{I}}(\bar{w}_{\mathrm{I}}), \tag{4.25}$$

where
$$G_{\mathrm{I}}=g_{\mathrm{I}}^{-1}, \tag{4.26}$$

and g_{I} is an as yet undetermined function of the indicated argument. However, the boundary condition (4.23) implies that

$$g_{\mathrm{I}}(\bar{w}_{\mathrm{I}})=-\bar{w}_{\mathrm{I}}[\xi_{\Delta}+\bar{w}_{\mathrm{I}}^2+\ln|\bar{w}_{\mathrm{I}}|]. \tag{4.27}$$

Notice that the inconvenient absolute value signs can now be omitted because the argument of the log term in (4.25) and (4.27) is $(\partial \bar{w}_{\mathrm{I}}/\partial \bar{\xi})/\bar{w}_{\mathrm{I}}$, which is always positive.

Solving for $\partial \bar{w}_{\mathrm{I}}/\partial \bar{\xi}$ and integrating the result with respect to $\bar{\xi}$ shows that $\bar{w}_{\mathrm{I}}$ is given by

$$\mu(\bar{z})+\int_{\mp\infty}^{\bar{w}_{\mathrm{I}}}\exp\left[-(\bar{z}/\tau)-\tau^2\right]\frac{\mathrm{d}\tau}{\tau}=-\exp\left[-\bar{\xi}+\xi_{\Delta}\right]\quad\text{for}\quad\bar{z}\gtrless 0, \tag{4.28}$$

where $\mu(\bar{z})$ is an arbitrary function of $\bar{z}$.

Substituting (4.28) into (4.19) now shows that $\bar{v}_{\mathrm{I}}$ is given by

$$\bar{v}_{\mathrm{I}}=1+\bar{w}_{\mathrm{I}}\exp\left[\bar{\xi}-\xi_{\Delta}\right]\left[\int_{\mp\infty}^{\bar{w}_{\mathrm{I}}}\exp\left[-(\bar{z}/\tau)-\tau^2\right]\frac{\mathrm{d}\tau}{\tau^2}-\mu'(\bar{z})\right], \tag{4.29}$$

and therefore, unlike the blending-layer velocity $\bar{v}_0$, remains finite at all points of space. However, it will exhibit exponential growth as $\bar{\xi}\rightarrow\infty$ unless $\mu(\bar{z})=\text{const.}$ More importantly, however (4.28) implies that

$$\bar{w}_{\mathrm{I}}\rightarrow\mp\bar{\xi}^{\frac{1}{2}}\quad\text{as}\quad\bar{\xi}\rightarrow+\infty\quad\text{for}\quad\bar{z}\gtrless 0, \tag{4.30}$$

when $$\mu(\bar{z}) \equiv 0. \tag{4.31}$$

In which case (4.9) and (4.22) show that (4.28) will match directly onto the blending-layer solution (3.16) as $\bar{\xi} \to +\infty$ and there will then be no need to introduce any intermediate regions to connect up the solutions. Two of us (M.E.G. and S.J.L.) believe this is the appropriate choice of μ (see figure 2). However, it follows from (4.28) that $\bar{w}_1$ will then be discontinuous across $\bar{z} = 0$ for any finite value of $\bar{\xi}$. Fortunately, this discontinuity decays like an exponential of an exponential of $\bar{\xi}$ and is therefore not incompatible with the upstream blending-layer solution, which is continuous across $\bar{z} = 0$. This does, however, suggest that there might be a very small $O(\exp\exp\bar{\xi})$ region where matching does not occur. This region can probably be eliminated by viscous effects. These issues will be pursued in a forthcoming paper. Notice that $\bar{v}_1$ will always be continuous across $\bar{z} = 0$ even though $\bar{w}_1$ like the external blending-layer solution, may be discontinuous there. However, it may be possible to eliminate this discontinuity by breaking the symmetry about $z = 0$.

5. The boundary-layer expansion

Viscous effects must also come into play when y becomes sufficiently small. The resulting boundary layer will initially be two dimensional with the crossflow effects producing only a linear perturbation (as in Toomre 1960) until its thickness becomes of the order of the lengthscale $\lambda\delta$ introduced in §3. We therefore suppose that $\bar{y} = O(1)$, introduce the long streamwise lengthscale

$$L^* = -\frac{\lambda}{\epsilon \ln \delta}, \tag{5.1}$$

and set $$\lambda\delta = \frac{L^*}{R^{\frac{1}{2}}}, \tag{5.2}$$

where $$R \equiv \frac{U_\infty L^*}{\nu} \tag{5.3}$$

is the 'global' Reynolds number based on L^*. It then follows that

$$\delta = \frac{1}{(R_\lambda \epsilon \ln[1/\delta])^{\frac{1}{2}}}, \tag{5.4}$$

which, in view of (2.1), is consistent with our assumption (3.1) that $\delta \ll 1$.

We first consider the region where $|\bar{x} - \xi_s| \gg \sigma$.

5.1. *The early three-dimensional region*

We expect the streamwise velocity

$$u = U(\bar{x}, \bar{y}, z) \tag{5.5}$$

to be $O(1)$ in this part of the flow and in order to satisfy continuity we put

$$v = -\epsilon\delta(\ln\delta)\, V, \tag{5.6}$$

$$w = -\epsilon(\ln\delta)\, W, \tag{5.7}$$

where V and W are, of course, assumed to remain $O(1)$ as $\epsilon \to 0$. Equations (3.3), (3.10) and (3.18) suggest that

$$p = \epsilon^2 \mathrm{d}(z) + O(\epsilon\delta \ln\delta)^2 \tag{5.8}$$

in this region.

Substituting these scalings into the Navier–Stokes equations yields the three-dimensional zero pressure gradient boundary-layer equations

$$U\frac{\partial U}{\partial \bar{x}}+V\frac{\partial U}{\partial \bar{y}}+W\frac{\partial U}{\partial z}=\frac{\partial^2 U}{\partial \bar{y}^2}, \tag{5.9}$$

$$U\frac{\partial W}{\partial \bar{x}}+V\frac{\partial W}{\partial \bar{y}}+W\frac{\partial W}{\partial z}=\frac{\partial^2 W}{\partial \bar{y}^2} \tag{5.10}$$

and

$$\frac{\partial U}{\partial \bar{x}}+\frac{\partial V}{\partial \bar{y}}+\frac{\partial W}{\partial z}=0. \tag{5.11}$$

U must clearly go to unity as $\bar{y}\to\infty$ in order to match with (3.7). The boundary condition for W is a bit more subtle. The known properties of the boundary-layer solutions suggest that the cross-stream derivatives should become small as $\bar{y}\to\infty$. Equation (5.10) therefore becomes

$$\frac{\partial W}{\partial \bar{x}}+W\frac{\partial W}{\partial z}=0, \tag{5.12}$$

whose solution is given by

$$W=G(z-\bar{x}W). \tag{5.13}$$

This will clearly agree with (3.16), and (5.7) will therefore match with (3.9) if we take

$$G=F, \tag{5.14}$$

where F is given by (3.18). It is worth noting that the continuity equation (5.11) automatically ensures that (5.6) will match with (3.8) and (3.14).

The appropriate boundary conditions for (5.9)–(5.11) are therefore

$$U\to 1, \quad W\to F(z-\bar{x}W) \quad \text{as} \quad \bar{y}\to\infty, \tag{5.15}$$

$$U=V=W=0 \quad \text{at} \quad \bar{y}=0 \tag{5.16}$$

and since the crossflow effects become small as $\bar{x}\to 0$, U must go to the Blasius solution in this limit, i.e.

$$U\to U_{\mathrm{B}}(\bar{x},\bar{y}) \quad \text{as} \quad \bar{x}\to 0. \tag{5.17}$$

The solution to this problem should, of course, become singular at the inviscid singular point ξ_{s}.

5.2. *Terminal form of early three-dimensional solution*

It is first necessary to find the terminal asymptotic form of the solution to the initial boundary-layer problem (5.9)–(5.11) in order to extend the boundary-layer solution through the singularity. For simplicity, we again consider only the case, corresponding to our numerical example, where the crossflow velocity vanishes at the singularity.

We expect the solution to be of similarity form in the vicinity of the singular point ξ_{s} and the numerical results suggest that it develops a double-layer structure with a thick, predominantly inviscid, outer region and a somewhat thinner viscous dominated sublayer. We therefore begin with the outer region, put

$$\tilde{y}=(\xi_{\mathrm{s}}-\bar{x})^{\gamma}\,\bar{y}, \tag{5.18}$$

and
$$\tilde{z} = \frac{z}{(\xi_s - \bar{x})^{\frac{3}{2}}}, \tag{5.19}$$

with $\gamma > 0$ and seek a solution of the form

$$U = f(\tilde{y}, \tilde{z}), \tag{5.20}$$

$$V = \frac{g(\tilde{y}, \tilde{z})}{(\xi_s - \bar{x})^{\gamma+1}}, \tag{5.21}$$

and
$$W = (\xi_s - \bar{x})^{\frac{1}{2}} h(\tilde{y}, \tilde{z}). \tag{5.22}$$

It follows from (5.9)–(5.11) that

$$-\tfrac{1}{2}fh + (g - \gamma\tilde{y}f)\frac{\partial h}{\partial \tilde{y}} + (h + \tfrac{3}{2}\tilde{z}f)\frac{\partial h}{\partial \tilde{z}} = 0, \tag{5.23}$$

$$(g - \gamma\tilde{y}f)\frac{\partial f}{\partial \tilde{y}} + (h + \tfrac{3}{2}\tilde{z}f)\frac{\partial f}{\partial \tilde{z}} = 0, \tag{5.24}$$

$$-\gamma\tilde{y}\frac{\partial f}{\partial \tilde{y}} + \frac{\partial g}{\partial \tilde{y}} + \tfrac{3}{2}\tilde{z}\frac{\partial f}{\partial \tilde{z}} + \frac{\partial h}{\partial \tilde{z}} = 0. \tag{5.25}$$

The value of γ may, in general, depend on the choice of upstream distortion u'_∞, but for the case, corresponding to our numerical example, where the singularity lies on a symmetry plane, h must behave like $h_0(\tilde{y})\tilde{z}$ as $\tilde{z} \to 0$ with the $\tilde{z}$-derivatives of f and g vanishing on this plane. It follows from (5.24) that either $\partial f/\partial \tilde{y}$ must vanish or

$$g = \gamma\tilde{y}f. \tag{5.26}$$

Our numerical results suggest the latter, and (5.25) therefore implies that

$$h_0 + \gamma f = 0, \tag{5.27}$$

which will only be compatible with (5.23) if

$$\gamma = 1, \tag{5.28}$$

which, in turn, shows that

$$h_0 = -f \quad \text{on} \quad \tilde{z} = 0. \tag{5.29}$$

Equations (3.7)–(3.9), (3.14) and (4.5)–(4.7) require that

$$f \to 1, \tag{5.30}$$

$$h \to \tilde{h}(\tilde{z}) \equiv -3\left(\frac{\beta_s}{3}\right)^{\frac{3}{2}} B\left(\frac{\tilde{z}}{2}\left(\frac{3}{\beta_s}\right)^{\frac{3}{2}}\right), \tag{5.31}$$

$$g \to -\tilde{y}h', \tag{5.32}$$

as $\tilde{y} \to \infty$, for all $-\infty < \tilde{z} < \infty$.

Upon eliminating $g - \gamma\tilde{y}f$ between (5.23) and (5.24) we find that h must be of the form

$$h = -\frac{3}{\tilde{H}(f)} B(\tfrac{1}{2}\tilde{z}\tilde{H}(f))f, \tag{5.33}$$

where B is defined by (4.8) and/or (4.9) and $\tilde{H}$ is an as yet undetermined function of f which, at least in our numerical example, remains bounded at $f = 0$ with

$$H_0 \equiv \tilde{H}(0) \neq 0. \tag{5.34}$$

The boundary condition (5.31) requires that

$$\tilde{H} \to \left(\frac{3}{\beta_s}\right)^{\frac{3}{2}} \quad \text{as} \quad f \to 1, \tag{5.35}$$

and expanding B for small $\tilde{z}$ shows that

$$h \to -\tilde{z}f \tag{5.36}$$

as $\tilde{z} \to 0$ with $\tilde{H} = O(1)$. The inviscid boundary condition at the plate requires that $g \to 0$ there, but our numerical solution suggests that the stronger, viscous type, condition

$$f \sim \tilde{y} \quad \text{as} \quad \tilde{y} \to 0 \tag{5.37}$$

actually holds at this point. We will show that there is a self consistent solution that satisfies this condition.

Eliminating $g - \gamma \tilde{y} f$ between (5.24) and (5.25) and substituting (5.33) into the result shows that f is determined by the nonlinear partial differential equation

$$f_{\tilde{y}} f_{\tilde{z}\tilde{y}} - f_{\tilde{z}} f_{\tilde{y}\tilde{y}} = \tfrac{1}{2}\tilde{H}\tilde{G}'(\tfrac{1}{2}\tilde{z}\tilde{H}) f_{\tilde{y}}^2, \tag{5.38}$$

where we have set $\gamma = 1$, put

$$\tilde{G}(\zeta) = \ln[B^2(\zeta) + 1], \tag{5.39}$$

and, as usual, the prime denotes differentiation with respect to the complete argument. It is easy to verify by inspection that (5.38) has a first integral of the form

$$\frac{\partial f}{\partial \tilde{y}} = [B^2(\tfrac{1}{2}\tilde{z}\tilde{H}) + 1]\,\tilde{F}(f), \tag{5.40}$$

where $\tilde{F}$ is an, as yet undetermined, function of f. Integrating with respect to $\tilde{y}$ shows that the solution to (5.38) that satisfies (5.37) is given by

$$\tilde{y} = \int_0^f \frac{\mathrm{d}f}{\tilde{F}(f)\,[B^2(\tfrac{1}{2}\tilde{z}\tilde{H}) + 1]}. \tag{5.41}$$

Equations (4.8) and (5.40) imply that

$$\tilde{F} = \left(\frac{\partial f}{\partial \tilde{y}}\right)_{\tilde{z}=0}, \tag{5.42}$$

which can be determined from the numerical solution on the symmetry plane, which in turn shows that $(\partial f/\partial \tilde{y})_{\tilde{z}=0}$ goes to a non-zero constant, say $\tilde{a}$ as $\tilde{y} \to 0$. It therefore follows from (5.24), (5.33), (5.34), (5.40) and (5.42) that

$$f \to \tilde{a}(1 + B_0^2)\,\tilde{y}, \quad g \to \tilde{a}\tilde{y}^2, \quad h \to -\frac{3}{H_0} B_0 f \tag{5.43}$$

as $\tilde{y} \to 0$ for all $-\infty < \tilde{z} < \infty$, where we have put

$$B_0 = B_0(\tilde{z}) \equiv B(\tfrac{1}{2}\tilde{z}H_0). \tag{5.44}$$

To find the 'viscous' wall-layer solution we put

$$\tilde{Y} \equiv (\xi_s - \bar{x})^{\alpha}\,\bar{y}, \tag{5.45}$$

and seek a similarity solution of the form

$$U = (\xi_s - \bar{x})^{1+2\alpha} F_w(\tilde{Y}, \tilde{z}), \tag{5.46}$$

$$V = (\xi_s - \bar{x})^{\alpha} G_w(\tilde{Y}, \tilde{z}), \tag{5.47}$$

$$W = (\xi_s - \bar{x})^{\frac{3}{2}+2\alpha} H_w(\tilde{Y}, \tilde{z}). \tag{5.48}$$

Matching with (5.43) requires that

$$F_w \sim \tilde{Y}, \quad G_w \sim \tilde{Y}^2, \tag{5.49}$$

as $\tilde{Y} \to \infty$, and consequently that

$$\alpha = 0. \tag{5.50}$$

It therefore follows from (5.9)–(5.11) and (5.45)–(5.48) that

$$-F_w^2 + G_w \frac{\partial F_w}{\partial \tilde{Y}} + (H_w + \tfrac{3}{2}\tilde{z}F_w)\frac{\partial F_w}{\partial \tilde{z}} = \frac{\partial^2 F_w}{\partial \tilde{Y}^2}, \tag{5.51}$$

$$-\tfrac{3}{2}F_w H_w + G_w \frac{\partial H_w}{\partial \tilde{Y}} + (H_w + \tfrac{3}{2}\tilde{z}F_w)\frac{\partial H_w}{\partial \tilde{z}} = \frac{\partial^2 H_w}{\partial \tilde{Y}^2}, \tag{5.52}$$

and

$$-F_w + \frac{\partial G_w}{\partial \tilde{Y}} + \tfrac{3}{2}\tilde{z}\frac{\partial F_w}{\partial \tilde{z}} + \frac{\partial H_w}{\partial \tilde{z}} = 0. \tag{5.53}$$

The viscous wall conditions require that

$$F_w = G_w = H_w = 0 \quad \text{at} \quad \tilde{Y} = 0. \tag{5.54}$$

The appropriate solution to this problem, i.e. the one that matches to (5.43), is given by

$$F_w = \tilde{a}(1 + B_0^2)\,\tilde{Y}, \quad G_w = \tilde{a}\tilde{Y}^2, \quad H_w = -\frac{3}{H_0} B_0 F_w. \tag{5.55}$$

It follows that the wall shear must behave like

$$\left(\frac{\partial U}{\partial \tilde{Y}}\right)_{\tilde{Y}} = \tilde{\tau}(\tilde{z})\,(\xi_s - \bar{x}) \quad \text{as} \quad \bar{x} \to \xi_s, \tag{5.56}$$

where

$$\tilde{\tau} \equiv \tilde{a}[1 + B^2(\tfrac{1}{2}\tilde{z}H_0)]. \tag{5.57}$$

5.3. *The inner boundary-layer solution*

Close to the singularity, where $\xi - \xi_s = O(\sigma)$, the boundary-layer solution must match onto the inner solutions (4.14)–(4.17) (rather than onto (3.20)) and onto the terminal forms (5.20)–(5.22) and/or (5.46)–(5.48) of the boundary-layer solutions (5.5)–(5.7). The simplest possible structure for this region will then involve two layers with an effectively constant-pressure upper-layer solution of the form

$$u = U_1(\hat{\xi}, \bar{y}_1, \hat{z}), \tag{5.58}$$

$$v = \frac{\epsilon\delta_1}{\sigma^2} V_1(\hat{\xi}, \bar{y}_1, \hat{z}), \tag{5.59}$$

$$w = \frac{\epsilon}{\sigma^{\frac{1}{2}}} W_1(\hat{\xi}, \bar{y}_1, \hat{z}), \tag{5.60}$$

and $$p = \epsilon^2 \mathrm{d}(z) + O(\epsilon\delta_{\mathrm{I}})^2,$$

where $$\bar{y}_{\mathrm{I}} \equiv \frac{y}{\delta_{\mathrm{I}}} = O(1), \tag{5.61}$$

$$\hat{\xi} \equiv \frac{\xi - \xi_{\mathrm{s}}}{\sigma} + \xi_{\mathrm{s}}(\ln \bar{y}_{\mathrm{I}} - \ln \xi_{\mathrm{s}}\sigma) = -(\bar{x} - \xi_{\mathrm{s}}) \ln y - \xi_{\mathrm{s}} \ln \xi_{\mathrm{s}} = O(1), \tag{5.62}$$

$$\hat{z} \equiv \frac{z}{\sigma^{\frac{3}{8}}} = O(1), \tag{5.63}$$

and, in order to match with (5.5)–(5.7) and (5.20)–(5.22) we must take

$$\delta_{\mathrm{I}} = \frac{\delta}{\sigma}. \tag{5.64}$$

Substituting these into the Euler equations (viscous effects are, of course, negligible on the short streamwise lengthscale (4.12) or (5.62)) we find that U_{I}, V_{I} and W_{I} still satisfy the three-dimensional inviscid, constant pressure boundary-layer equations (but now in terms of the inner variables $\hat{\xi}$, $\bar{y}_{\mathrm{I}}$, and $\hat{z}$) which means that W_{I} and U_{I} are related by

$$\hat{g}(W_{\mathrm{I}}, U_{\mathrm{I}}) = \frac{U_{\mathrm{I}}\hat{z}}{W_{\mathrm{I}}} - \hat{\xi} + \frac{1}{3}\left(\frac{\tilde{H}W_{\mathrm{I}}}{3U_{\mathrm{I}}}\right)^2, \tag{5.65}$$

where $\hat{g}$ is an arbitrary function of the indicated arguments that is ultimately determined by the boundary conditions and the $(\tilde{H}W_{\mathrm{I}}/3U_{\mathrm{I}})^2$ term, which could have been incorporated into $\hat{g}$, has been inserted for convenience. U_{I} can, at least in principle, be determined by solving (5.65) for W_{I} and substituting the result into the continuity equation with V_{I} eliminated via one of the momentum equations.

Matching with the free-stream solution in (4.14) requires that

$$U_{\mathrm{I}} \to 1 \quad \text{as} \quad \bar{y}_{\mathrm{I}} \to \infty, \tag{5.66}$$

and, since $U_{\mathrm{I}} - 1$, W_{I}, and $(1/\bar{y}_{\mathrm{I}})\,W_{\mathrm{I}\hat{\xi}}$ all satisfy the same perturbed momentum equation when $U_{\mathrm{I}} \to 1$, it follows that U_{I} and W_{I} can be expressed as functions of $(1/\bar{y}_{\mathrm{I}})\,W_{\mathrm{I}\hat{\xi}}$ when $\bar{y}_{\mathrm{I}} \to \infty$ and therefore that we can choose $\hat{g}$ so that

$$\hat{g} \to \xi_{\mathrm{s}}\left[\ln\left(\frac{\xi_{\Delta}}{\bar{y}_{\mathrm{I}}}\frac{W_{\mathrm{I}\hat{\xi}}}{W_{\mathrm{I}}}\right) - \xi_{\Delta}\right] \quad \text{as} \quad \bar{y}_{\mathrm{I}} \to \infty. \tag{5.67}$$

Equation (5.65) will then match onto the free-stream solution (4.16), (4.25) and (4.27) while matching with the upstream solution (5.20) and (5.22) requires that $\hat{g}$ remain bounded and

$$U_{\mathrm{I}} \to f\left(-\hat{\xi}\bar{y}_{\mathrm{I}}, \frac{\hat{z}}{(-\hat{\xi})^{\frac{3}{8}}}\right), \tag{5.68}$$

as $\hat{\xi} \to -\infty$ and/or $\hat{z} \to \pm\infty$ (see (4.9)).

The inviscid expansions (5.58)–(5.60) are again invalid in the near wall region where $\bar{y}_{\mathrm{I}} \to 0$. However, the scalings (5.62) and (5.63) should still hold and the upstream solutions (5.46)–(5.48) suggest that u and w will be $O(\sigma)$ and $O(\sigma^{\frac{1}{2}}\epsilon)$, respectively, there. The viscous terms will then be of the same order as the

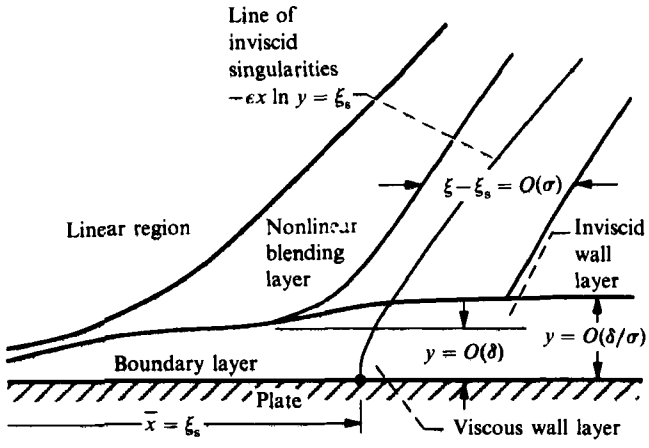

FIGURE 3. Overview of asymptotic structure.

convection terms when $\bar{y} = O(1)$ and it follows from the requirements of continuity that the wall-layer solution should scale like

$$u = \sigma \bar{U}_{\mathrm{I}}(\hat{\xi}, \bar{y}, \hat{z}), \tag{5.69}$$

$$v = \frac{\epsilon\delta}{\sigma} \bar{V}_{\mathrm{I}}(\hat{\xi}, \bar{y}, \hat{z}), \tag{5.70}$$

$$w = \epsilon\sigma^{\frac{1}{2}} \bar{W}_{\mathrm{I}}(\hat{\xi}, \bar{y}, \hat{z}). \tag{5.71}$$

Then it follows from the Navier–Stokes equations that the order-one quantities $\bar{U}_{\mathrm{I}}, \bar{V}_{\mathrm{I}}, \bar{W}_{\mathrm{I}}$ are again determined by the viscous wall condition (5.16) and the zero pressure gradient boundary-layer equations (5.9)–(5.11) (but now with $\hat{\xi}$ and $\hat{z}$ in place of $\bar{x}$ and z).

Matching with the upstream solutions (5.46)–(5.48) requires that,

$$\bar{U}_{\mathrm{I}} \to -\hat{\xi}\tilde{a}(1 + B_0^2)\,\bar{y}, \tag{5.72}$$

$$\bar{W}_{\mathrm{I}} \to -\frac{3}{H_0}(-\hat{\xi})^{\frac{3}{2}} \tilde{a} B_0 (1 + B_0^2)\,\bar{y}, \tag{5.73}$$

etc., as $\hat{\xi} \to -\infty$.

The upper- and lower-layer solutions must, of course, match to each other in some overlap domain $\bar{y}_{\mathrm{I}} \to 0$, $\bar{y} \to \infty$ with $\hat{\xi} = O(1)$. This will only occur if $U_{\mathrm{I}} \sim \bar{y}_{\mathrm{I}}$ as $\bar{y}_{\mathrm{I}} \to 0$, which actually turns out to be the case. However, this in itself does not guarantee that matching and/or solvability will occur and it may be necessary to introduce some intermediate region and/or pressure variations to complete the solution. We do not pursue this further, but merely mention that the problem can be solved in closed form and leave the details to a forthcoming report.

Figure 3 summarizes the overall asymptotic structure of the problem developed in this and the preceding sections.

6. Numerical solution of the boundary-layer problem

Numerical solutions to the full three-dimensional boundary-layer problem (5.9)–(5.11), (5.17) and (5.16) were obtained using the Keller box method (Keller & Cebeci 1972; Cebeci & Smith 1974; Cebeci, Khattab & Stewartson 1981). This finite-difference procedure advances the solution in $\bar{x}$ and z from given initial conditions

and an independent symmetry-plane calculation. With an appropriate choice for the upstream distortion (such as the one described in §7) the marching in z can proceed from the symmetry plane at $z = -\pi$ to the one at $z = 0$. In the absence of any crossflow reversal the standard box (Cebeci *et al.* 1981) was found to be adequate. The Blasius solution is the appropriate initial condition at $\bar{x} = 0$.

Since the boundary layer becomes very thick near the singularity in the external inviscid solution, the stretched transverse variable

$$\tilde{\eta} = \left[1 - \frac{(z+\pi)}{\pi}\bar{x}\right]\frac{\bar{y}}{\bar{x}^{\frac{1}{2}}} \tag{6.1}$$

was introduced. Then, following the standard procedure, the boundary-layer equations are written as a system of first-order differential equations

$$\left.\begin{aligned} p' + ep &= \frac{\bar{x}}{\left[1 - \frac{(z+\pi)}{\pi}\bar{x}\right]^2}\left(U\frac{\partial U}{\partial \bar{x}} + W\frac{\partial U}{\partial z}\right), \\ q' + eq &= \frac{\bar{x}}{\left[1 - \frac{(z+\pi)}{\pi}\bar{x}\right]^2}\left(U\frac{\partial W}{\partial \bar{x}} + W\frac{\partial W}{\partial z}\right), \end{aligned}\right\} \tag{6.2}$$

$$U' = p, \quad W' = q \tag{6.3}$$

$$e' = \frac{1 + \frac{z+\pi}{\pi}\bar{x}}{2\left[1 - \frac{(z+\pi)}{\pi}\bar{x}\right]^3}U + \frac{1}{\pi}\frac{\bar{x}^2}{\left[1 - \frac{(z+\pi)}{\pi}\bar{x}\right]^3}W + \frac{\bar{x}}{\left[1 - \frac{(z+\pi)}{\pi}\bar{x}\right]^2}\left(\frac{\partial U}{\partial \bar{x}} + \frac{\partial W}{\partial z}\right) \tag{6.4}$$

where $' \equiv \partial/\partial\tilde{\eta}$.

The boundary conditions are given by (5.15)–(5.17) and

$$e(\bar{x}, \tilde{\eta} = 0, z) = 0. \tag{6.5}$$

A non-uniform mesh is used in the cross-stream coordinate such that the J mesh points are distributed according to

$$\tilde{\eta}_0 = 0; \quad \tilde{\eta}_j = h_1\frac{K^j - 1}{K - 1}, \quad j = 1, J. \tag{6.6}$$

This has the effect of increasing the local mesh size from its smallest value near the wall, h_1, by a fixed percentage (prescribed by the constant K) for each subsequent box.

The introduction of the finite-difference approximations yields a nonlinear system of equations for the unknown variables at the next (streamwise or spanwise) cross-grid point. The nonlinear system is linearized about a previous iteration (or initial guess) by Newton's method. The difference between two iterations is solved for in an efficient way by the block tridiagonal procedure until convergence is achieved.

7. Results and discussion

Since vorticity is carried by the fluid particles in an inviscid flow, vortex lines that are perpendicular to the plate at upstream infinity become infinitely elongated as they pass over the plate leading to infinite velocities and infinitesimal lengthscales

that can only be eliminated by viscous effects. This vortex stretching produces the logarithmic singularity in the initial linear inviscid solution which, incidentally, is well known in classical rapid-distortion-theory literature (Hunt & Carruthers 1990). There is also a much more interesting nonlinear singularity that develops further downstream in the flow and leads to the formation of small spanwise lengthscales. It results from the fact that the large spanwise velocity field diminishes the effect of the horizontal pressure gradients to the point where the spanwise velocity is a purely convected quantity to lowest approximation. Its convective nature is quite similar to the unsteady separation singularities studied by Cowley, Van Dommelen & Lam (1990) and by Russell & Landahl (1984).

The blending-layer singularity causes the vertical (or upwash) velocity to become infinite along a line

$$\bar{x}\eta = \xi_s = \text{const.} \tag{7.1}$$

in the $(z = 0)$-plane (see figure 2) with the spanwise velocity solution (3.16) being discontinuous across the portion of the plane extending downstream of this line. The upwash singularity is eliminated by a local asymptotic solution (constructed in §4) that fully couples the spanwise and vertical velocity fields but allows the downstream discontinuity to extend into the local asymptotic region surrounding the singularity.

We have seen that the blending-layer solution involves a function F that is related to the (imposed) upstream distortion field, i.e. u_∞, by (3.18) with the constant a being determined by the local potential flow in the vicinity of the forward stagnation point. The latter can easily be scaled out of the blending-layer problem as well as the wall boundary-layer problem, to be discussed below, by replacing ϵ by $a\epsilon$ in (5.1), (5.4), (5.6) and (5.7).

Our interest is primarily in periodic disturbance fields and, for definiteness, we choose

$$u_\infty = -\cos z, \tag{7.2}$$

in which case the initial singularity will lie at

$$\xi_s = 1. \tag{7.3}$$

The choice (7.2) has special symmetry properties which may make some of our results (particularly those for the boundary layer to be discussed below) less than universal. However, this issue is beyond the scope of the present work and will be discussed in a 'follow-on' paper.

Figure 4 is a plot of the scaled crossflow streamline patterns within the inviscid blending layer as calculated from (3.14) and (3.16). They show that the blending-layer flow is just the lower portion of the large streamwise vortices that reside at an $O(1)$ distance from the wall. The streamlines are tangent to the symmetry plane when $\bar{x} < 1$ because the crossflow velocity vanishes there, but they intersect the symmetry plane over a finite range of η when $\bar{x} > 1$ owing to the previously described discontinuity in the solution (3.16) for $\bar{w}_0$. The region of intersection first appears at the wall (i.e. $\eta = 1$) when $\bar{x} = 1$ and then spreads out over a finite range of η as $\bar{x}$ increases downstream. This suggests that the boundary layer will separate from the wall at $\bar{x} = 1$.

The streamlines also intersect the wall at $\eta = 1$, but, as will be shown below, this streamline pattern is smoothly turned around by the viscous boundary-layer flow to form the bottom of the vortex pattern. This is possible because the physical (i.e. unscaled) η-velocity is much smaller than the spanwise velocity and can therefore match onto the small upwash velocity at the edge of the viscous boundary layer.

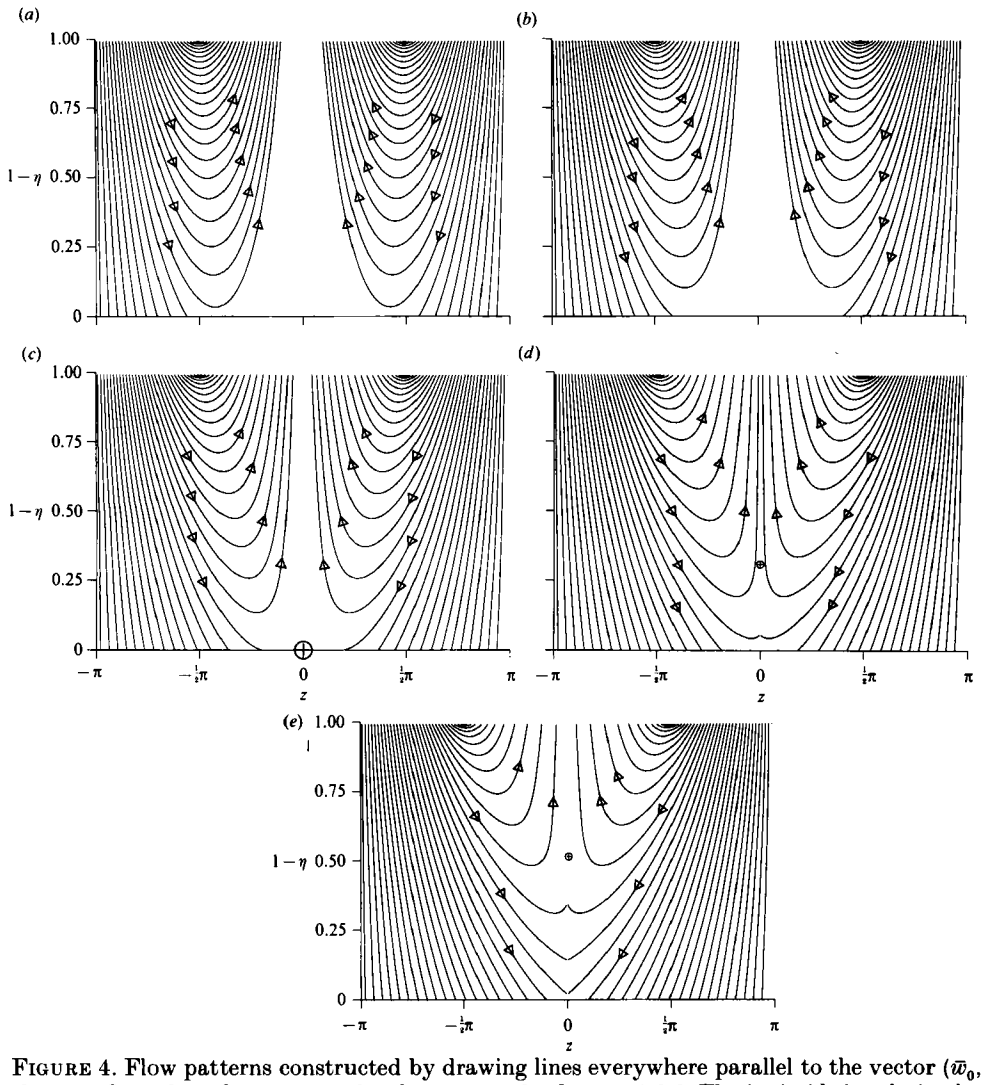

FIGURE 4. Flow patterns constructed by drawing lines everywhere parallel to the vector $(\bar{w}_0, \bar{v}_0)$ in the crossflow plane for $\bar{x} =$ (*a*) 0.25, (*b*) 0.5, (*c*) 1.0, (*d*) 1.5, (*e*) 2.0. The inviscid singularity location is marked with ⊕. Arrows denote flow direction.

The characteristic streamwise lengthscale L^* of the boundary-layer flow is given by

$$L^* = -\frac{2\lambda a}{\epsilon \ln (R_\lambda \epsilon)^{\frac{1}{2}}}, \tag{7.4}$$

when L^* is renormalized to absorb a into the scaling. The boundary-layer singularity therefore develops on this scale, which means that it occurs further downstream (relative to the characteristic lengthscale λ of the disturbance) as the characteristic amplitude ϵ of the upstream disturbance and the leading-edge/disturbance scale Reynolds number R_λ decrease. R_λ must, of course, always remain large in order for our analysis to be valid. The effect of the leading-edge geometry is accounted for by the factor a.

The upstream boundary-layer flow is predominantly two dimensional and there is an overlap region (in which $\bar{x} \ll 1$ and $x \gg 1$) where it is given by the Blasius solution.

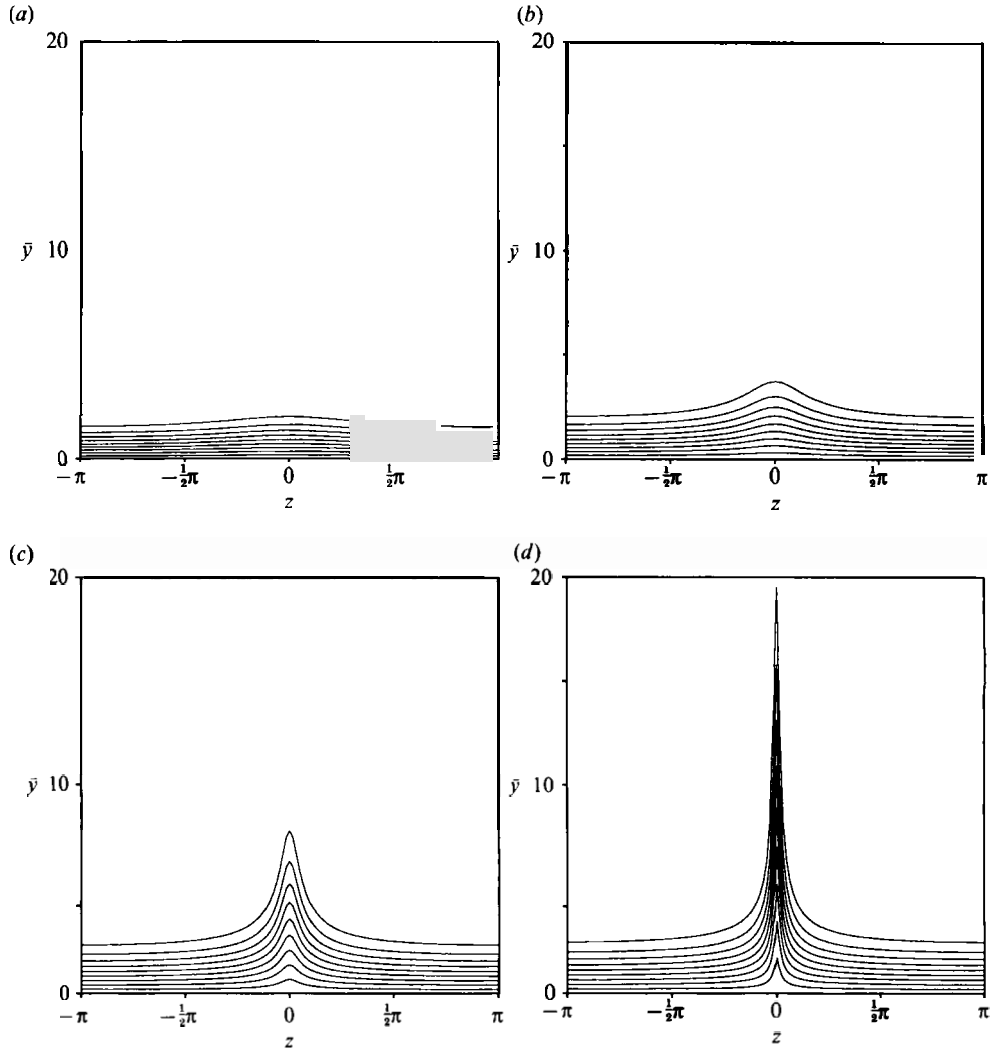

FIGURE 5. Streamwise velocity contours in crossflow plane for $\bar{x}$ = (*a*) 0.25, (*b*) 0.5, (*c*) 0.75, (*d*) 0.9. The levels shown are, from top to bottom, U = 0.9, 0.8, 0.7, 0.6, 0.5, 0.4, 0.3, 0.2, 0.1.

This solution is therefore the appropriate upstream boundary condition for the $\bar{x}$-scale boundary-layer problem under discussion. Contours of the computed streamwise velocity in the crossflow plane are shown at a number of streamwise positions in figure 5. They show the gradual development of spanwise variations in the velocity profiles with increasing downstream distance. The most significant effects occur near the symmetry plane, which lies at $z = 0$. These results clearly show the anticipated localized thickening of the boundary layer in this region and the associated reduction in spanwise lengthscale.

Benney (1984) was among the first to show that asymptotically small modulations occurring on sufficiently short lengthscales can lead to order-one changes in the mean flow. However, Benney's modulations arose from interacting instability waves and are fundamentally different from the steady upstream distortion effects being considered herein.

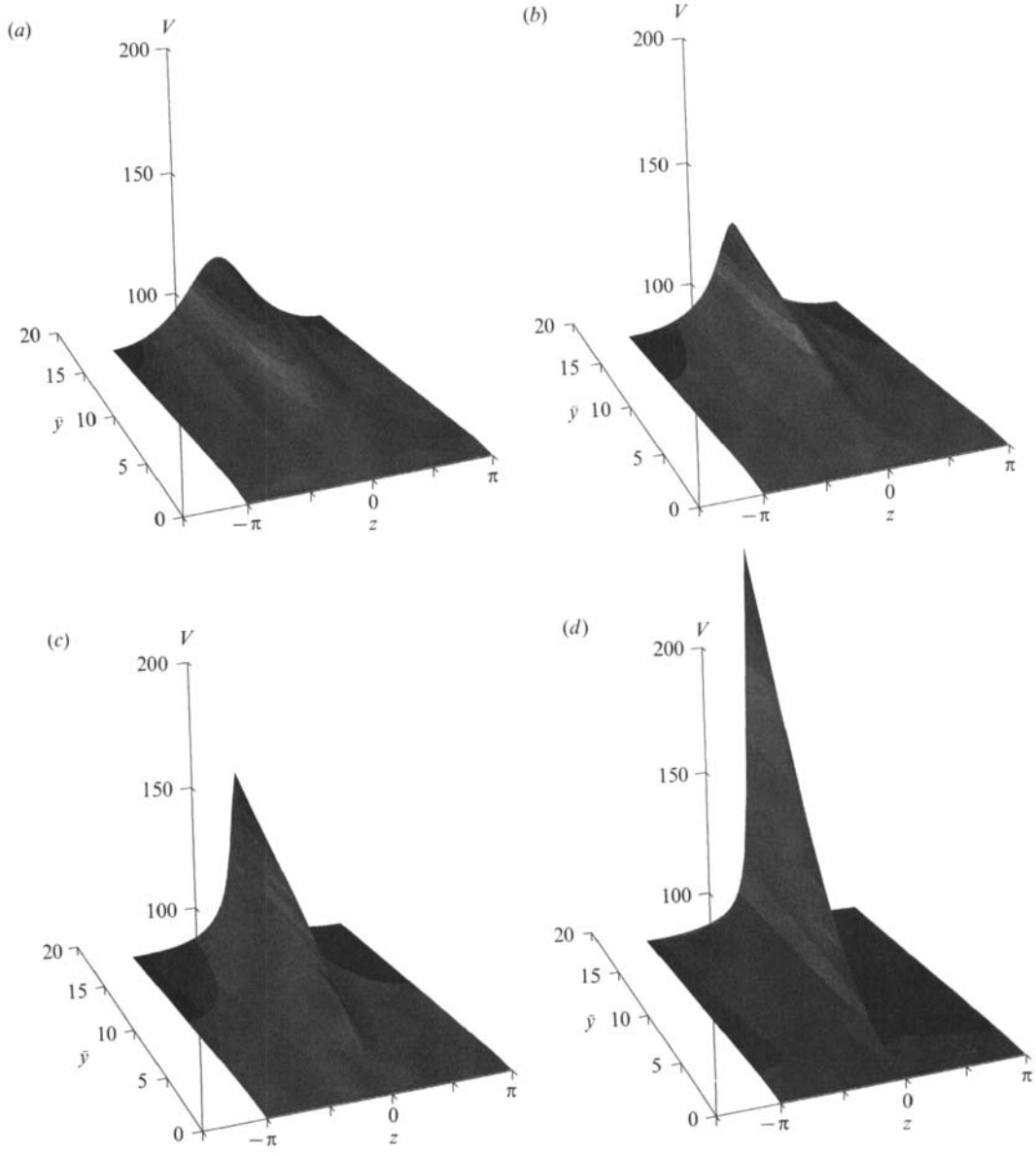

FIGURE 6. Upwash velocity profiles as a function of $\bar{y}$ and z for $\bar{x} =$ (*a*) 0.25, (*b*) 0.5, (*c*) 0.75, (*d*) 0.9.

Figure 6 is a plot of the corresponding upwash velocity profiles. It shows that the upwash velocity becomes very large in the vicinity of the symmetry plane $z = 0$ as $\bar{x} \to 1$. The dramatic local increase in this velocity component might be described as a kind of 'bursting phenomenon' which, up to now, has primarily been associated with unsteady flows. This might lead to a local transition of the boundary layer and therefore provide a possible mechanism for by-pass transition. The answer to this question depends on the stability of the solution to the local rescaled boundary-layer problem of §5.3. The final resolution of this issue is therefore beyond the scope of the present work but will be pursued in a forthcoming paper.

The velocity vectors in the crossflow $(z, \bar{y})$-plane at the same streamwise stations

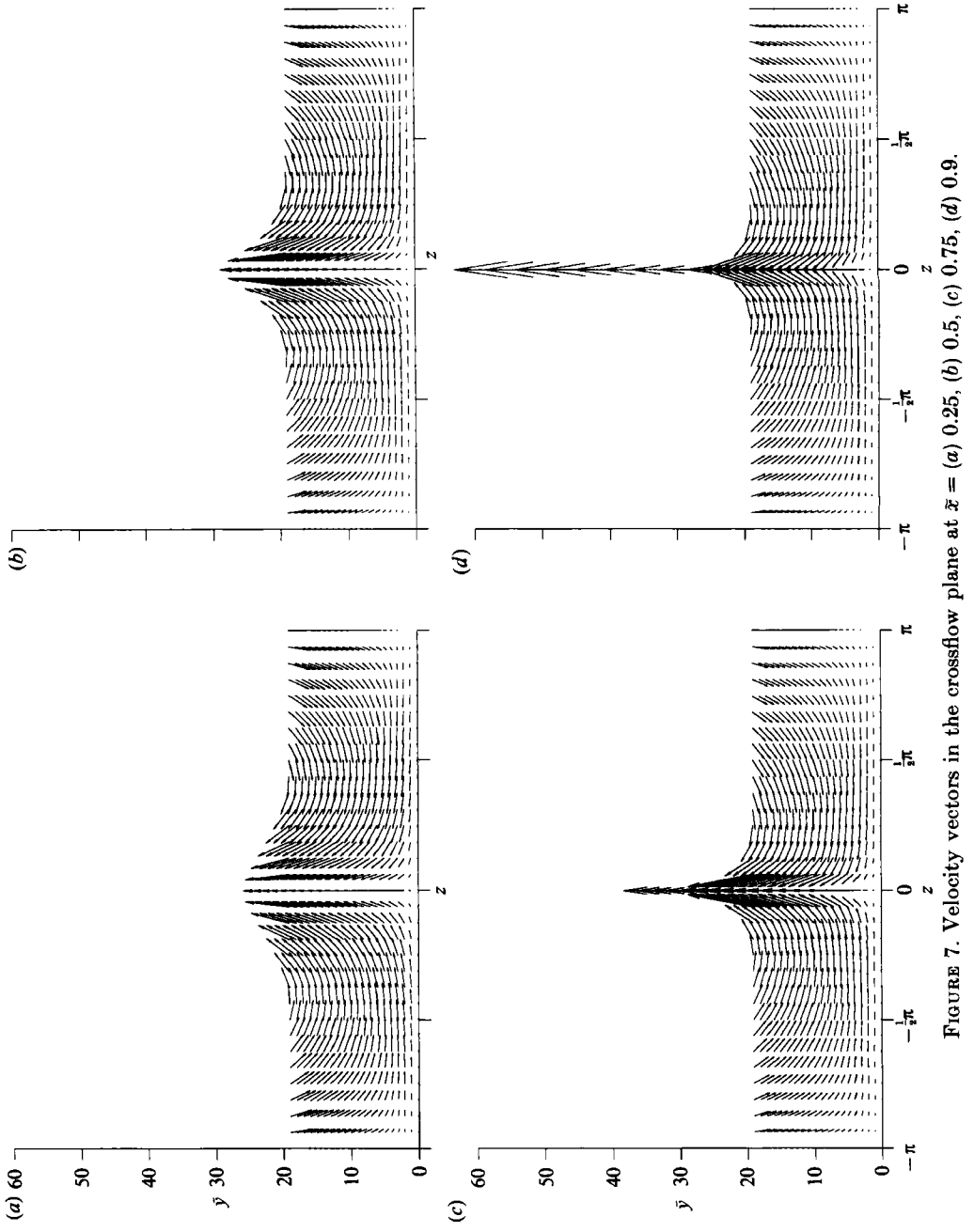

FIGURE 7. Velocity vectors in the crossflow plane at $\bar{x} =$ (*a*) 0.25, (*b*) 0.5, (*c*) 0.75, (*d*) 0.9.

are plotted in figure 7. They show that the large upwash velocity is produced by a spanwise flow into the symmetry plane.

The analysis of §5.2 shows that the boundary-layer solution develops a double-layer structure with the terminal form of this solution given by (5.20)–(5.22), (5.26), (5.33) and (5.41) in the upper inviscid region whose thickness increases like

$$\frac{1}{1-\bar{x}} \quad \text{as} \quad \bar{x} \to 1, \tag{7.5}$$

and by (5.46)–(5.48) and (5.55) in the lower viscous region, whose thickness remains $O(1)$ as $\bar{x} \to 1$. The solution in this region is identical to the limiting asymptotic form of the solution in the upper region so that the lower layer is not a distinct asymptotic region but is part of the upper inviscid region to thc order of approximation of the analysis.

The solution becomes particularly simple on the symmetry plane where it implies that

$$U = f(\tilde{y}, 0), \tag{7.6}$$

$$\frac{\mathrm{d}W}{\mathrm{d}z} = -\frac{f(\tilde{y}, 0)}{(1-\bar{x})}, \tag{7.7}$$

and

$$V = \frac{\tilde{y} f(\tilde{y}, 0)}{(1-\bar{x})^2}, \tag{7.8}$$

where the function f is indeterminate and has to be found from the numerical solution. The solution in the lower layer is still given by these formulae but with f equal to its asymptotic form

$$f = \tilde{a}\tilde{y}, \tag{7.9}$$

where $\tilde{a}$ is a constant.

The numerical results of figures 5–7 are in qualitative agreement with this terminal asymptotic solution of the three-dimensional boundary-layer problem. This includes the local thickening of the boundary layer at the symmetry plane, the development of a short spanwise lengthscale, and the development of a very large upwash velocity.

To obtain an accurate quantitative check on our terminal asymptotic solution we worked out the numerical solution to the symmetry plane boundary-layer equations starting from the upstream Blasius solution. These equations can, of course, be solved independently of the flow in the rest of the boundary layer and are much simpler than the full three-dimensional equations. It turns out that (7.7) and (7.8) constitute an exact solution to these full equations and still satisfy the correct free-stream boundary condition, so that the numerical problem is especially simple in this case.

Figure 8(*a*) is a plot of the symmetry plane streamwise velocity profiles (at various values of $\bar{x}$) as a function of the composite singularity coordinate $\bar{y}(1-\bar{x})/\bar{x}^{\frac{1}{2}}$. It merely shows that the profiles go smoothly from their initial Blasius to their final asymptotic forms. Figure 8(*b*) shows that these profiles look quite different when plotted against the unscaled coordinate $\bar{y}$ and again reflects the dramatic thickening of the boundary layer. The predicted linear behaviour at the wall is also evident from this figure. The calculated wall shear stress is shown in figure 9. The asymptotic linear behaviour and the ultimate vanishing of the wall shear, predicted by (5.56), is clearly verified by these results.

To check the terminal asymptotic solution off the symmetry plane, we compare the results of the full three-dimensional computation with the asymptotic similarity solution.

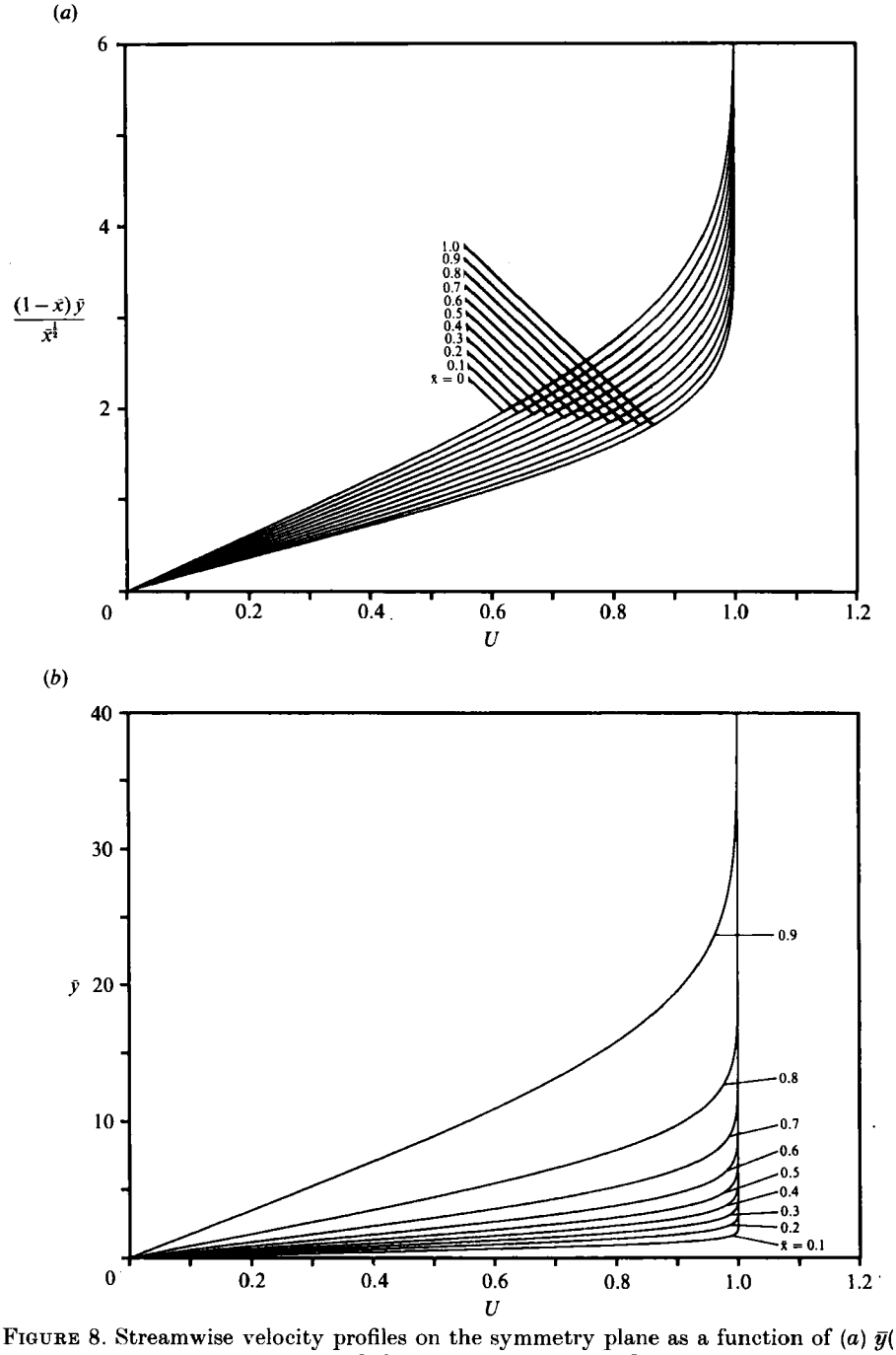

FIGURE 8. Streamwise velocity profiles on the symmetry plane as a function of (*a*) $\bar{y}(1-\bar{x})/\bar{x}^{\frac{1}{3}}$, and (*b*) $\bar{y}$ at various values of $\bar{x}$.

The asymptotic solution requires that the crossflow velocity tends to (5.31) at the outer edge of the boundary layer. Figure 10 shows a comparison of $\tilde{h}$ as determined from (5.31) with curves obtained from numerically computed solutions of the inviscid Burgers' equation (equation (5.15)) with (7.2) at a number of $\bar{x}$ positions. The latter is the boundary condition used for the crossflow velocity in the numerical

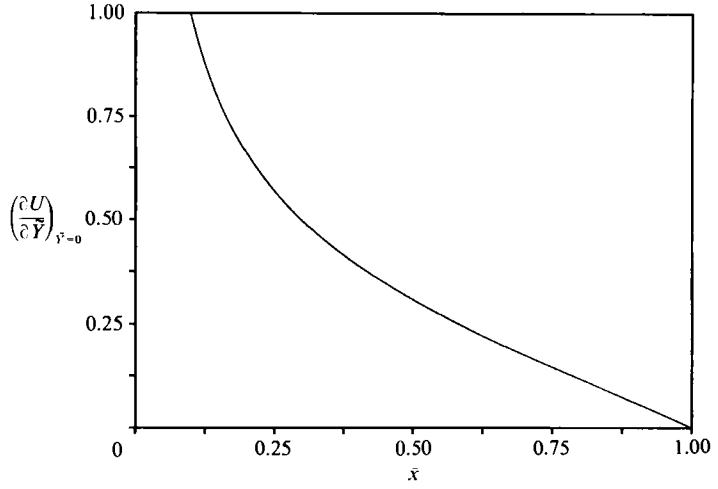

FIGURE 9. Wall shear on symmetry plane as a function of $\bar{x}$.

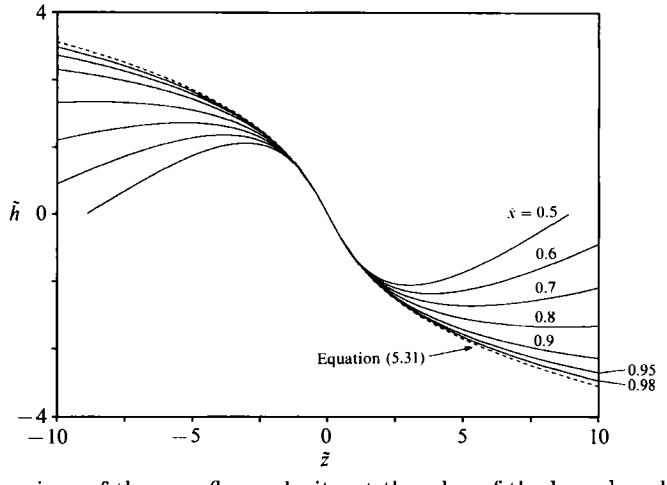

FIGURE 10. Comparison of the crossflow velocity at the edge of the boundary layer from ——, numerical solution and – – –, equation (5.31).

computation. Figure 10 shows that the solutions first agree with (5.31) for $\tilde{z}$ near zero (the symmetry plane) and that agreement is attained over a broader range in $\tilde{z}$ as $\bar{x}$ gets closer to 1. This comparison gives an indication of the ranges over which we can expect the numerically computed boundary-layer solution to agree with the asymptotic similarity solution.

Figure 11 is a comparison of the calculated wall stress $\tilde{\tau}$ with results obtained from (5.57) with $\tilde{a}$ determined from the slope of the symmetry plane wall shear curve in figure 9 and H_0 taken to be 2.1.

A similar comparison for the spanwise wall shear

$$\left(\frac{\partial W}{\partial \tilde{Y}}\right)_{\tilde{Y}=0} = \tilde{\sigma}(\tilde{z})\,(\xi_s - \bar{x})^{\frac{3}{2}} \quad \text{as} \quad \bar{x} \to \xi_s, \tag{7.10}$$

where

$$\tilde{\sigma}(\tilde{z}) = -\frac{3\tilde{a}}{H_0} B(\tfrac{1}{2}\tilde{z}H_0)\,[1 + B^2(\tfrac{1}{2}\tilde{z}H_0)], \tag{7.11}$$

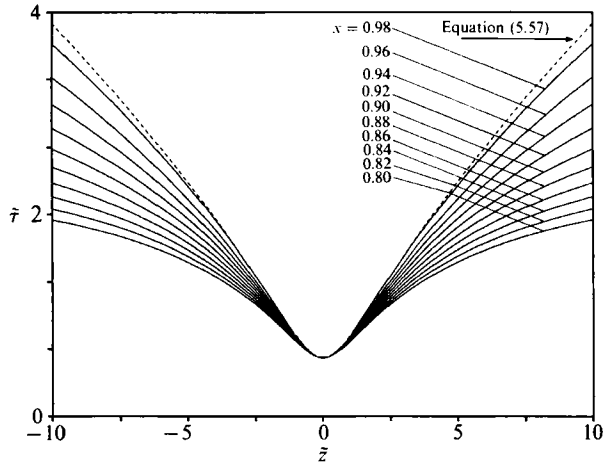

FIGURE 11. Comparison of the streamwise wall shear stress from ——, numerical solution and – – –, asymptotic similarity solution.

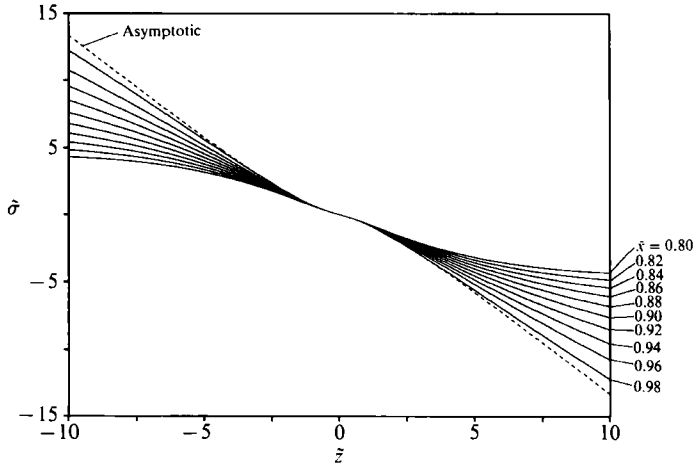

FIGURE 12. Comparison of the spanwise wall shear stress from ——, numerical solution and – – –, asymptotic similarity solution.

is shown in figure 12. These results suggest that the asymptotic behaviour is first achieved near $\tilde{z} = 0$ and spreads out away from the symmetry plane as $\bar{x}$ gets closer to 1. It is worth noting that $\tilde{\tau}$ has its minimum at $\tilde{z} = 0$ while the spanwise shear is linear there.

The vanishing of the wall shear at $\bar{x} = 1$ is indicative of the formation of a singularity in the boundary-layer solution at this point. But the fact that this singularity is directly attributable to a removable singularity in the outer inviscid solution strongly suggests that it is basicaly inviscid in nature and that it too may be removable. The final resolution of this issue requires a solution to the local rescaled boundary-layer problem of §5.3, which is beyond the scope of the present work. The non-removability of the singularity would require that the upstream flow field predicted by our analysis be modified owing to some form of boundary-layer separation that would have to be accounted for in the initial formulation of the inviscid flow problem. This separation, which is definitely of the boundary-layer

collision type, might be similar to the 'open' separation found by Stewartson, Cebeci, & Chang (1980) (see also Stewartson & Simpson 1982). It could, of course, be eliminated by terminating the plate before the singularity had a chance to form. Even if this is not done the local decrease in wall shear stress could promote instability and transition upstream of the singularity and again modify the flow before the singularity can occur.

Finally, we note that the present study bears some resemblance to the receptivity analysis of Goldstein (1983, 1985), Goldstein, Sockol & Sanz (1983) and Goldstein, Leib & Cowley (1987) in that it involves the internalization of free-stream disturbances with an attendant streamwise amplification of the perturbed boundary-layer flow, but it differs from them in that it only involves changes in the mean flow and does not depend on the growth of local instability waves to produce the final effect.

The authors would like to thank Professor A. F. Messiter of the University of Michigan for helpful discussions during the course of this work.

Appendix

In this Appendix we investigate the singular behaviour of the drift function in the vicinity of the forward stagnation point where the complex potential $\tilde{W}$ behaves like

$$\tilde{W} \sim -\tfrac{1}{2}aZ^2, \tag{A 1}$$

and a is a real constant that is determined by matching with the 'outer' potential flow. It therefore follows from (2.5) that

$$\zeta = -aZ = -(-2a\tilde{W})^{\frac{1}{2}}, \tag{A 2}$$

and, consequently, that

$$|\zeta|^2 = 2a(\Phi^2 + \Psi^2)^{\frac{1}{2}}. \tag{A 3}$$

Hence

$$\int \frac{\mathrm{d}\Phi}{|\zeta|^2} = \int \frac{\mathrm{d}\Phi}{U_0^2 + V_0^2} \sim \frac{1}{2a}\int \frac{\mathrm{d}\Phi}{(\Phi^2+\Psi^2)^{\frac{1}{2}}} = -\frac{1}{2a}\ln\left[(\Phi^2+\Psi^2)^{\frac{1}{2}} - \Phi\right]. \tag{A 4}$$

It follows that

$$\Delta \sim -\frac{1}{a}\ln\Psi \quad \text{as} \quad \Psi \to 0 \quad \text{when} \quad \Phi > 0. \tag{A 5}$$

REFERENCES

AGRAWAL, S. & MESSITER, A. F. 1984 Turbulent boundary-layer interaction with a shock wave at a compression corner. *J. Fluid Mech.* **143**, 23–46.

AMES, W. F. 1965 *Nonlinear Partial Differential Equations*. Academic.

BENNEY, D. J. 1984 The evolution of disturbances in shear flows at high Reynolds numbers. *Stud. Appl. Maths* **70**, 1–19.

BUSH, W. B. 1971 On the Lagerstrom mathematical model for viscous flow at low Reynolds number. *SIAM J. Appl. Maths* **20** (2), 279–287.

CEBECI, T., KHATTAB, A. K. & STEWARTSON, K. 1981 Three-dimensional laminar boundary layers and the OK of accessibility. *J. Fluid Mech.* **107**, 57–87.

CEBECI, T. & SMITH, A. M. O. 1974 *Analysis of Turbulent Boundary Layers*. Academic.

COWLEY, S. J., VAN DOMMELEN, L. L. & LAM, S. T. 1990 On the use of Lagrangian variables in descriptions of unsteady boundary layer separation. *ICASE Rep.* no. 90–47.

CROW, S. C. 1966 The spanwise perturbation of two-dimensional boundary layers. *J. Fluid Mech.* **24**, 153–164.

DARWIN, C. 1953 A note on hydrodynamics. *Proc. Camb. Phil. Soc.* **49**, 342–354.

GOLDSTEIN, M. E. 1978 Unsteady vortical and entropic distortions of potential flows round arbitrary obstacles. *J. Fluid Mech.* **89**, 433–468.

GOLDSTEIN, M. E. 1979 Turbulence generated by the interaction of entropy fluctuations with non-uniform meanflows. *J. Fluid Mech.* **93**, 209–224.

GOLDSTEIN, M. E. 1983 The evolution of Tollmien–Schlichting waves near a leading edge. *J. Fluid Mech.* **127**, 59–81.

GOLDSTEIN, M. E. 1985 Scattering of acoustic waves into Tollmien–Schlichting waves by small streamwise variations in surface geometry. *J. Fluid Mech.* **154**, 509–529.

GOLDSTEIN, M. E., LEIB, S. J. & COWLEY, S. J. 1987 Generation of Tollmien–Schlichting waves on interactive marginally separated flows. *J. Fluid Mech.* **181**, 485–517.

GOLDSTEIN, M. E., SOCKOL, P. M. & SANZ, J. 1983 The evolution of Tollmien–Schlichting waves near a leading edge. Part 2. Numerical determination of amplitudes. *J. Fluid Mech.* **129**, 443–453.

HUNT, J. C. R. & CARRUTHERS, D. J. 1990 Rapid distortion theory and the 'problems' of turbulence. *J. Fluid Mech.* **212**, 497–532.

KELLER, H. B. & CEBECI, T. 1972 Accurate numerical methods for boundary layer flows. *AIAA J.* **10**, 1193–1199.

LAGERSTROM, P. A. & CASTEN, R. G. 1972 Basic concepts underlying singular perturbation techniques. *SIAM Rev.* **14** (1), 63–120.

LANDAHL, M. T. 1990 On sublayer streaks. *J. Fluid Mech.* **212**, 243.

LIGHTHILL, M. J. 1956 Drift. *J. Fluid Mech.* **1**, 31–53.

RUSSELL, J. M. & LANDAHL, M. T. 1984 The evolution of a flat eddy near a wall in an inviscid shear flow. *Phys. Fluids* **27**, 557–570.

STEWARTSON, K., CEBECI, T. & CHANG, K. C. 1980 A boundary-layer collision in a curved duct. *Q. J. Appl. Maths* **33**, 59–75.

STEWARTSON, K. & SIMPSON, C. J. 1982 On a singularity initiating a boundary-layer collision. *Q. J. Mech. Appl. Maths* **35**, 1–16.

TOOMRE, A. 1960 The viscous secondary flow ahead of an infinite cylinder in a uniform parallel shear flow. *J. Fluid Mech.* **7**, 145–155.